Annu. Rev. Phys. Chem. 1990. 41:15–60

ULTRAFAST MOLECULAR REACTION DYNAMICS IN REAL-TIME: Progress Over a Decade

Lutfur R. Khundkar[1] *and Ahmed H. Zewail*

Arthur Amos Noyes Laboratory of Chemical Physics,[2] California Institute of Technology, Pasadena, California 91125

KEY WORDS: ultrafast chemistry, femtosecond chemistry, reaction dynamics, IVR, transition states.

INTRODUCTION

One of the goals of researchers in the field of reaction dynamics is to develop an understanding of the elementary steps involved in a chemical reaction on a molecular level (see e.g. Ref. 1). The century-old Arrhenius rate law, a phenomenological description of the temperature dependence of rates of reactions in bulk, has been used extensively to deduce activation energies and frequency factors. The activated complex theory (also referred to as absolute rate theory or transition-state theory, see e.g. Refs. 2, 3) postulated more than 50 years ago, provides a useful interpretation of the Arrhenius rate parameters in terms of molecular properties. These parameters contain practical information about rates, but they do not express the molecular details of a reaction. At this juncture, two types of questions can be raised—one concerning the effects of the environment on rates in condensed media, and the other, the purely molecular aspects of reactions in the absence of an environment, i.e. in an isolated molecular system. We restrict our attention to the latter case for the purposes of this review.

[1] Present address: Department of Chemistry, Northeastern University, Boston, Massachusetts 02115.

[2] Contribution No. 8090.

0066–426X/90/1101–0015$02.00

The fundamental physical issues in this field of *molecular* reaction dynamics are (*a*) how do initial conditions affect the outcome of a chemical reaction? (*b*) how is the excess energy partitioned among the various quantum states of the products? and (*c*) how does the system evolve from reactants to products? The basic approach is deeply rooted in scattering theory: If the initial conditions are precisely defined, and the interaction potential is well-known, then one can, in principle, predict the outcome of the reactive process precisely. Generally, the initial conditions and final product states can be experimentally determined. The potential energy, a function of many variables, is deduced indirectly, by making informed guesses and checking for consistency with experimental results (1).

Experimental studies of reactions thus face the challenge of defining the initial conditions precisely, as well as the detection of products with quantum state resolution. Two technological advances that have helped revolutionize experimental chemical kinetics are lasers and supersonic molecular beams. A large body of results has accumulated over the past three decades involving the characterization of such "before" (reagent) and "after" (product) observables and has led to a deeper understanding of reactive processes (1, 4–6). In addition to the large number of crossed molecular beams and chemiluminescence studies, an expanding literature of crossed molecular beam–laser results has probed dynamics via careful analyses of product internal energy (vibrational and rotational) distributions and steady-state alignment and orientation of products (1, 7–19). Approximate lifetimes of the collision (or half-collision) complexes and rates of the reactions have been derived from measurements of the steady-state angular distribution or alignment, and from linewidths of spectroscopic transitions in a number of cases (1, 4–21).

Time-resolved measurements of intramolecular dynamics offer an opportunity to observe a molecular system in the continuous process of its evolution from reactants to products. Under this rather general picture, one may further distinguish among intramolecular vibrational-energy redistribution (IVR), rates of chemical reactions on a state-to-state basis, and the dynamics of transition-state species. Generally, the timescale for IVR is on the order of picoseconds, and rates for predissociation are tens of picoseconds and longer. The "lifetime" of transition-state species is even shorter—femtoseconds—corresponding to subangstrom fragment displacements.

IVR in isolated molecules (22, 23) is a description of how energy initially localized in a specific type of vibrational motion is shared among all other types of nuclear motion possible. It has been shown that this process is a manifestation of the loss of quantum coherence imposed on the initial state via the preparation process, i.e. the coherence of the excitation pulse.

When a large number of states and couplings are involved, the average effect of redistribution can be described in terms of simple kinetics and rate constants (22, 23). The relevance of IVR to reaction dynamics lies in a possible reduction of the dimensionality of the general problem. If IVR is fast and complete, then the reaction is characterized by the energy and total angular momentum. Under these conditions, the reaction is said to be statistical (see e.g. 24) and statistical theories of reaction rates (25–31) may be applied; a reaction rate constant can be directly obtained from the exponential loss of population in the initial state or buildup in any product state. On the other hand, if the rate of reaction is intrinsically faster than the rate of energy redistribution, then one would expect the outcome of the reaction to be deterministic—initial state influences both rate and product distributions. A single rate constant cannot be defined and all possible combinations of initial and final quantum states would have to be considered for a complete description of the reaction.

Implicit in the above description is the existence of very short-lived ($\leq 10^{-12}$ seconds) transitional states between reactants and products. As reagents proceed to products during a reaction, the spectral properties of the system also evolve from being characteristic of reagents to those of "transition states" and eventually to being characteristic of the products. When the process of transition is continuous, the evolution of the spectra should also be continuous. Conventional spectroscopic methods should reveal the existence of nonstationary, or perturbed, species that correspond to transitional configurations. The overall effect is extremely small, however, and scales essentially with the "lifetime" of each such species. Since the lifetime is $\leq 10^{-12}$ s, the use of ultrashort pulses offers a distinct advantage in the study of such species. In some sense, these pulses provide a window of observation that discriminates against long-lived species and enhances the probability of detecting transitory species.

In the following sections we describe the techniques and some of our experimental results on the different topics discussed in general terms above: IVR, state-to-state rates, and femtosecond transition-state spectroscopy (FTS)—the tool for "femtochemistry." The focus is on *real-time* measurements of intramolecular dynamics, with special emphasis on reactive processes. We have attempted to highlight the underlying physical issues in each section, illustrating them with a number of examples, rather than attempt a comprehensive review of each topic (see 23, 32–34).

EXPERIMENTAL METHODOLOGY

Several apparatuses have been used in these experiments (32–39), and we present only an outline of the basic approach (Figure 1). For measurements

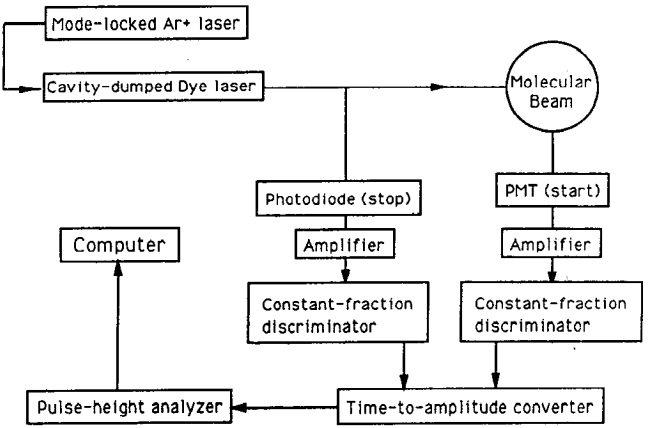

Figure 1a

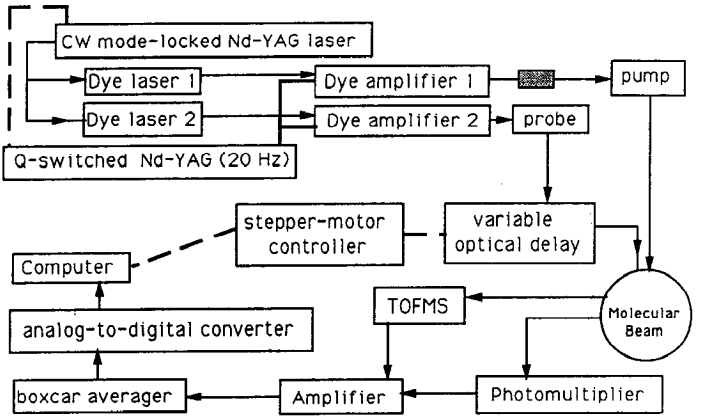

Figure 1b

Figure 1 Schematic diagram for the three major apparatuses developed for studies of ultrafast molecular reaction dynamics in real-time: (*a*) time-correlated single photon counting/molecular beam apparatus; (*b*) picosecond photofragment spectroscopy/molecular beam apparatus (LIF/MPI); (*c*) femtosecond transition-state spectroscopy apparatus. The *shaded blocks* on the pump (and similarly for the probe) are to indicate the many nonlinear methods used to generate different wavelengths.

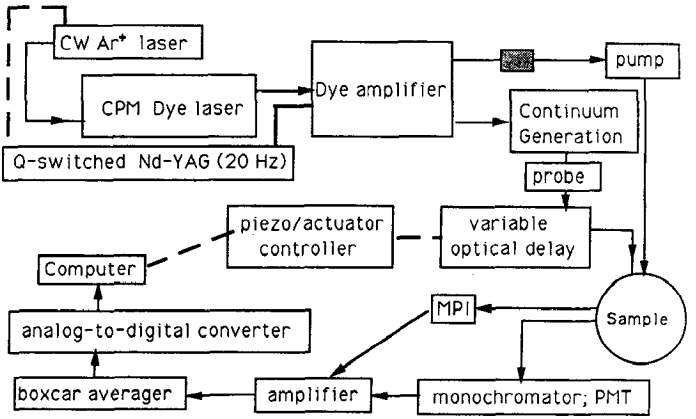

Figure 1c

of IVR, a picosecond pulse is used to create the initial state. Fluorescence or absorption from this initial state is resolved on the picosecond time scale (23, 35–39). Time-correlated single photon counting or pump-probe methods are used for measuring state-to-state rates. The pump-probe method employs two independently tunable pulsed lasers. This allows one to measure reagent decay and product rise-times as a function of the initial energy and the final product rotational, vibrational, or electronic quantum state. The two pulses, delayed in time and overlapped in space, are focused in the sample, either a low pressure gas or a supersonic beam of inert gas seeded with the molecule of interest. One of the pulses, the pump, is resonant with a transition in the reagent molecule, while the other, the probe, selectively excites or ionizes either a product or the excited reactant. The temporal evolution of the species selected by the probe is mapped out as the delay time between the two pulses is varied.

For the FTS (32–34) studies, the wavelength of the probe pulse is chosen to be in resonance with either the transition-states or the states of free products. The system may either fluoresce or be ionized after absorbing the probe pulse. Detection is made by laser induced fluorescence (LIF) or by multiphoton ionization (MPI). The latter is possible because intense ultrashort pulses are used. When the sample is seeded in a molecular beam, the ions can be identified with a mass-spectrometer built into the molecular beam apparatus. The temporal resolution of these methods is determined by the correlation width of the pump and probe pulses. The pulses themselves may be of the order of a few picoseconds or 40–100 femtoseconds, the lower limit ($\sim$6 fs) being set by the current state of ultrafast laser

technology (40). The spectral resolution is determined by the frequency spectrum of the pulses, generally close to the uncertainty limit.

STUDIES OF IVR IN REAL-TIME

Intramolecular vibrational-energy redistribution has been a topic of much interest among laser chemists for the past two decades. The interest stems from the hope that if enough energy can be localized in a bond for a period of time longer than the reaction time, one can achieve selective bond-fission (see e.g. 41, 42). For example, such selectivity has been observed in the UV photodissociation of bromoiodomethane (43), where the excitation of an electron from a nonbonding orbital on the halogen atom to the antibonding carbon-halogen bond yields either I or Br atoms, depending on the photolysis wavelength, rather than fission of the weakest bond in the molecule. So, what determines the selectivity and what is the time scale for energy redistribution?

Although the theory used to describe IVR is similar to that used for other nonradiative processes (internal conversion, intersystem crossing), IVR is distinct from these processes in that the electronic quantum number does not change (23). This field has been reviewed recently (22, 23); we highlight the principles and present a few illustrative examples drawn from our own studies (23).

Let us consider first the case of two-coupled-vibrational-levels, the simplest one in which the full details of IVR can be demonstrated (44). Thus we have the ground state ($|g\rangle$), a vibrationally excited level in the ground-state ($|f\rangle$), and two zero-order excited states ($|a\rangle$ and $|b\rangle$) (Figure 2), one of which ($|a\rangle$) is active in absorption and emission to the ground state, while $|b\rangle$ is active only in emission to $|f_b\rangle$. The two states $|a\rangle$ and $|b\rangle$ are coupled by the matrix element V_{ab}, giving rise to molecular eigenstates, $|1\rangle$ and $|2\rangle$. This coupling is determined by the anharmonicity of the potential and/or Coriolis interactions.

At time zero, the excitation process creates the superposition state $|\psi\rangle \sim |a\rangle$, which then evolves under the influence of the molecular Hamiltonian. The states are:

$$|1\rangle = \alpha|a\rangle + \beta|b\rangle \qquad 1a.$$

$$|2\rangle = \beta|a\rangle - \alpha|b\rangle \qquad 1b.$$

$$|\psi(t)\rangle = (\alpha|1\rangle e^{-iE_1 t/\hbar} + \beta|2\rangle e^{-iE_2 t/\hbar}) e^{-\Gamma t/2} \qquad 2.$$

where E_1 and E_2 are the energies of the two eigenstates and Γ^{-1} is the fluorescence lifetime. Thus the probability amplitude oscillates back and

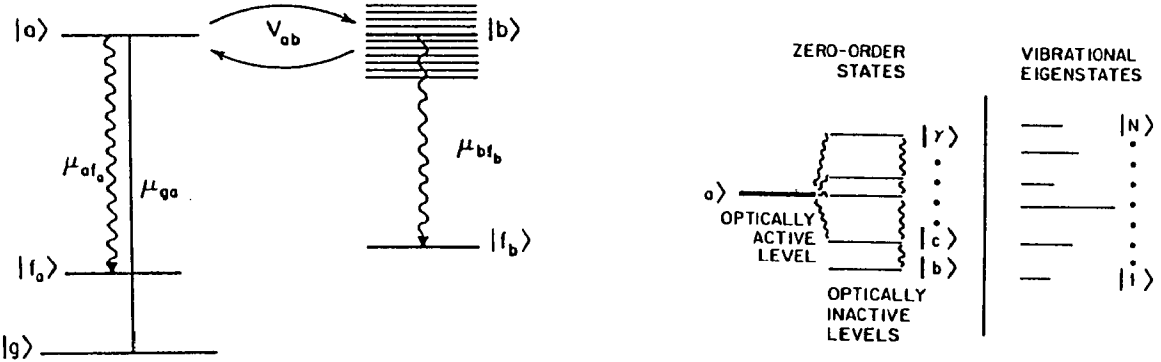

Figure 2 Conceptual representation of IVR in real-time. *Left*: level diagram for two, coupled zero-order states. $|a\rangle$ is active in absorption from the ground state, $|g\rangle$, and in emission to $|g\rangle$ and the level $|f_a\rangle$. $|b\rangle$ is active only in emission to the state $|f_b\rangle$. *Right*: the N coupled levels system. The zeroth-order $|a\rangle$ state on the left couples to the dark states $|b\rangle, |c\rangle, \ldots, |\gamma\rangle$ to give rise to the vibrational eigenstates $|1\rangle, |2\rangle, \ldots, |N\rangle$. The different lengths of the lines representing the eigenstates are supposed to signify the difference in absorption strengths for each eigenstate from $|g\rangle$.

forth between the initially excited superposition $|\psi\rangle$ and one orthogonal to it. Clearly, if we were to excite purely $|1\rangle$ or purely $|2\rangle$, a situation that can arise when the laser bandwidth is much narrower than the energy difference $E_1 - E_2$, the temporal behavior would be a simple exponential decay corresponding to fluorescence to the ground state. The key to determining experimental conditions that allow one to observe IVR (i.e. evolution of superposition states) lies in the detection wavelength. Since a given excited rovibrational state can emit to many different rovibrational states of the ground electronic state, the emission wavelength provides an extra degree of freedom that can be used to select a particular superposition of excited states (23). For instance, the time-dependent fluorescence from $|\psi(t)\rangle$ to the ground state is proportional to its overlap with $|a\rangle$:

$$|\langle a|\psi(t)\rangle|^2 = e^{-\Gamma t}[1 - 2\alpha^2\beta^2 + 2\alpha^2\beta^2 \cos(|E_1 - E_2|t/\hbar)], \quad 3.$$

whereas that to $|f_b\rangle$ is of opposite phase

$$|\langle b|\psi(t)\rangle|^2 = e^{-\Gamma t}[2\alpha^2\beta^2(1 - \cos(|E_1 - E_2|t/\hbar))]. \quad 4.$$

This simple picture of coupled oscillators gives us an intuitive feeling for the process of IVR, and although it is somewhat of an ideal case, experimental observations of such elementary redistribution processes in large polyatomic molecules have been made in this laboratory (see Figure 3 and Ref. 23). One sees that if both time and energy resolution of fluorescence (or absorption) are introduced, then IVR can be directly observed through the in-phase ("energy leaving") and out-of-phase ("energy receiving") detection of energy flow. The transients give the effective coupling matrix elements, in this case $2V_{ab} = E_1 - E_2$, as dictated by Eqs. 3 and 4.

From the discussion above, it follows that IVR becomes important when the density of states is large. This happens in all polyatomic molecules at high energies. In large molecules, the density is high even at low energies ($\sim$1000 cm^{-1}). Thus a consideration of the effects of IVR as a function of the number of coupled states is indicated. When many states are coupled (i.e. involved in the initial coherent state), the evolution is a complicated function of the energy spacing between participating states, and the loss of coherence can appear exponential (or quasi-exponential).

The overall behavior of IVR can be categorized into three types (23, 45–47): (*a*) no IVR, where only molecular eigenstates are excited; (*b*) restricted IVR, where $\sim$2–10 states are involved and quantum coherence effects (e.g. Eqs. 3 and 4) are observed; and (*c*) dissipative IVR where more than 10 states are involved and decays are observed (the total density of states could be much higher!). In Figure 4, we show results on anthracene as a function of excess energy as an example of the different types of behavior where the time scales (>18 ns to 22 ps) for the different regimes

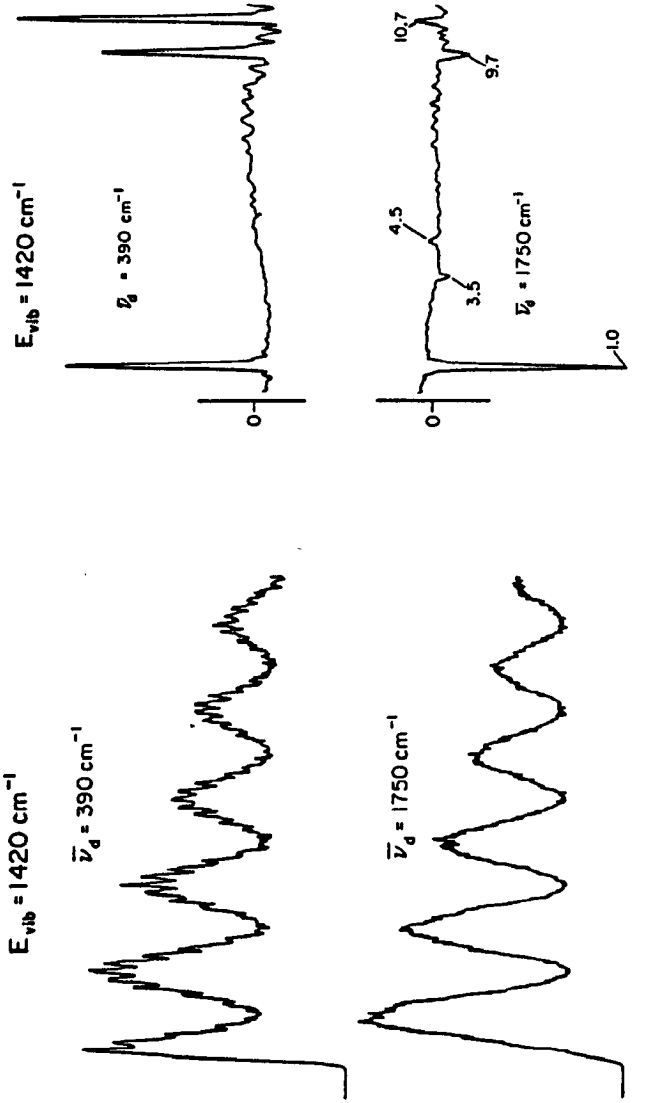

Figure 3 Experimental manifestation of IVR in real-time. Representative fluorescence decays show in-phase and out-of-phase quantum beats in emission from the 1420 cm^{-1} level of anthracene seeded in a beam. The $\bar{\nu}_d$ values are the shifts (in wavenumbers) of the detection energy from the excitation. The traces on the *right* are the Fourier transform of each transient. Some of the relevant frequencies are indicated on the figure which shows the number of vibrational levels coupled at the given vibrational energy (see 23).

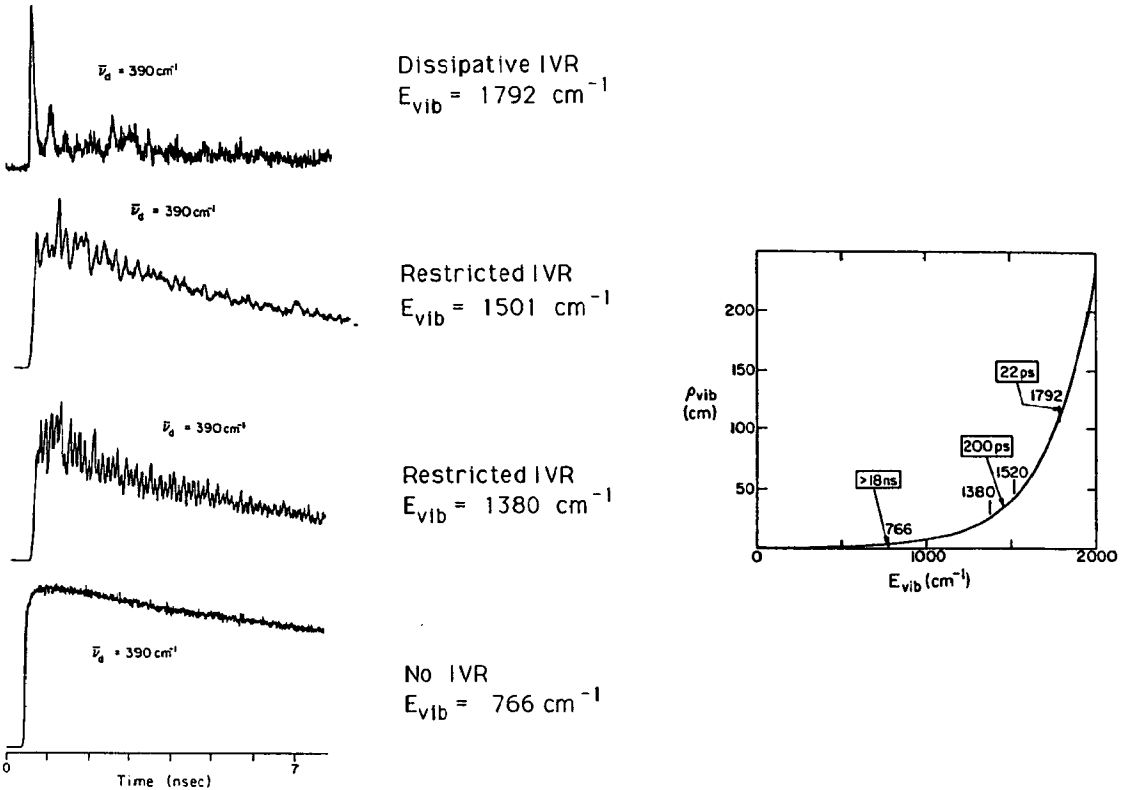

Figure 4 Three regimes of IVR: no IVR, restricted IVR, and dissipative IVR observed in a beam of anthracene. The traces on the *left* show the actual transient observed while detecting emission to the $\nu_{ex}-390$ cm^{-1} band. The plot on the *right* shows the increase in density of states as a function of energy and the timescales for IVR (see 23, 45–47).

have been established; restricted IVR occurs between 700–1300 cm^{-1} and dissipative IVR is seen for energies greater than 1700 cm^{-1} in S_1. Other molecules in which the dynamics of IVR has been studied include stilbene (48), deuterated analogs of anthracene and stilbene (49, 50), alkyl-substituted anthracenes (51), diphenyl-butadiene (52), pyrazine and perdeutero-pyrazine (53–55), isoquinoline (56, 57), *n*-alkyl anilines (58), *p*-difluorobenzene (59), azulene (60), 1-methylindole (61), pyrimidine (62), indole (63), tetrazene-Ar (see section on state-to-state microcanonical rates, below), perylene (64), naphthol (65), and fluorene (see section on purely rotational coherence, below). In a few of these examples, the vibrational redistribution involves some interstate electronic coupling (pyrazine, pyrimidine, isoquinoline).

High-resolution linewidth and spectral measurements, particularly on benzene (66) and pyrazine (67, 68), and "chemical timing" spectral studies on *p*-difluorobenzene and *p*-fluorotoluene (22), have contributed greatly to the study of IVR in these large molecules but are not reviewed here. It is important to emphasize that in relatively simple systems, where the eigenstates can be resolved, real-time studies of IVR and spectral analyses are complementary. In larger systems, however, spectral congestion is a serious problem and inferences of rates of IVR from spectral data could be misleading, as exemplified in the case of many molecules (see e.g. 45–47, 58, 59). Furthermore, care should be taken in translating linewidth measurements into rates of IVR because of inhomogeneous broadening and pure dephasing processes (23). Recent theoretical calculations by Marcus (69, 70) and Mukamel (71, 72) have reproduced features of the spectra and the observed quantum coherence effects in the restricted region of IVR. It is a challenge to be able to predict the threshold for restricted and dissipative IVR regions in large molecules with the density of states reaching 10^4 to 10^6 states per cm^{-1}.

In the quantum model of dissipative IVR, one finds that a complete rephasing of all the vibrational states occurs at some long time after excitation. These recurrence times can be much longer than the time scale of the experiment. Also note that both the excitation and the detection processes are important in observing IVR. In particular, if one can detect the total fluorescence, the effects of redistribution on a single electronic surface are "washed out," and one observes only incoherent decay corresponding to fluorescence (23). A final point that should be noted is the concept of complete redistribution. We have mentioned criteria for when IVR is not present, restricted or dissipative. Within this prescription, even when IVR is dissipative, it may be incomplete—a situation that occurs when some of the energetically accessible molecular eigenstates have no transition moment connecting them to the ground states populated in the

unexcited ensemble. In other words, dissipative IVR does not necessarily imply that all zero-order dark states are coupled to the initially excited state. In such cases, optical excitation cannot produce a uniform distribution in phase space, a common assumption in all statistical rate theories, and reactive dynamics may show features that do not follow the predictions of these theories.

ALIGNMENT EFFECTS IN REAL-TIME

Purely Rotational Coherence

The description of vibrational-energy redistribution presented in the previous section has been extended to include coherence among rotational states as well. The disparity in the timescales of vibrational (femtoseconds) and rotational (picoseconds to nanoseconds) motion in molecules leads to a natural separation of these effects. In other words, the effects appear distinct because the rotational motion of a molecule may be adequately represented as that of an equivalent molecule whose atoms are frozen in their equilibrium position (rigid-body approximation). The energy differences between rotational states are (nearly) commensurable and the predicted recurrence times are on the order of the timescale of our measurements. Therefore both the initial loss of coherence and subsequent rephasings can be observed in the polarized emission or absorption from a sample excited by a polarized laser source.

Although a quantum mechanical description of this phenomenon has been discussed in Refs. (73–75), a classical model based on the characteristics of rotation of a rigid body is useful as a convenient way of visualizing these coherences (76, 77). For illustration, we consider the case of a prolate symmetric top whose moments of inertia are I_a about the symmetry axis and I_b about some other axis perpendicular to it. The rotation of this object can be described as the combination of precession of the symmetry axis about the direction of the angular momentum, **J**, and a top-like spinning motion about this axis. The precession angular frequency, ω_1, is given by

$$\omega_1 = \frac{|\mathbf{J}|}{I_b} = 4\pi BJ, \qquad 5.$$

while the angular frequency of the motion about the top-axis, ω_2 is given by

$$\omega_2 = |\mathbf{J}| \cos\theta \left(\frac{1}{I_a} - \frac{1}{I_b}\right) = 4\pi(A-B)K. \qquad 6.$$

Here, J is the magnitude of the angular momentum and K is its projection on the symmetry axis. A and B are the rotational constants and θ is the precession angle. Figure 5 shows two positions of the rotating object half a nutation period apart in time. Since the initial pulse partially aligns the ensemble, it follows that for parallel transitions a total rephasing of dipoles occurs at the fundamental nutation frequency ($2B$) (assuming that J and K take on integer values only), since all molecules nutate at some multiple of that frequency (76). For perpendicular transitions, rephasings occur at $4(A-B)$, which is twice the fundamental rotation frequency, as well as the fundamental nutation frequency $2B$. Recurrences in fluorescence or absorption intensities associated with these two patterns of dipole rephasings constitute the principal observable consequences of pure rotational

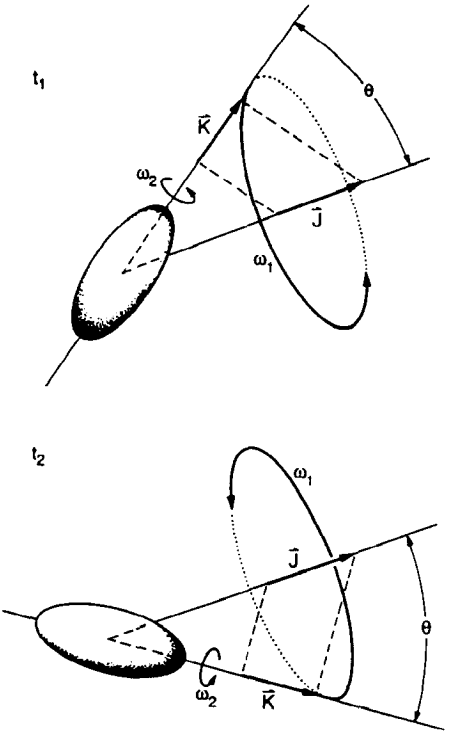

Figure 5 Classical rotational motion of a rigid symmetric top. The top is shown at two times separated by half a nutation period, ω_1 and ω_2 are the angular frequencies of nutation and of rotation about the symmetry axis, respectively. $\vec{J}$ is the total angular momentum vector and $\vec{K}$ is its component along the symmetry axis (see Ref. 76).

coherence in symmetric tops (and asymmetric tops) as discussed in Ref. (76). These effects have been observed in emission in supersonic beams (73–76), in resonance enhanced multiphoton ionization (78), and in fluorescence depletion (79, 80). Rotational coherence has also been treated and studied in gases near room temperature (77). Representative spectra are shown in Figure 6. It should be noted that rotational states can also participate (see e.g. 81–84) in IVR, e.g. by Coriolis coupling, an issue that has not been covered here.

From Eqs. 5 and 6 and Refs. (73–76), one can see that the recurrence time provides excited state rotational constants with Doppler-free resolution, a powerful feature of this technique (73–76). So far, this real-time method has been applied to stilbene (73–76, 78), anthracene (76), fluorene (76, 80) and iodine (see below). Within the limits of the accuracy of these measurements (typically better than 0.1%), they have been used to deduce the molecular structure of the excited states. This is particularly important for assigning structures to weakly bound clusters, as demonstrated for rare gas clusters of stilbene and fluorene (76).

Polarized Photofragment Spectroscopy

The discussion in the preceding section has been focused on nonreactive systems. Here, we extend it to photofragmentation processes. The asymptotic (steady-state) anisotropy, difference in photofragment yields as observed with the probe light source polarized parallel and perpendicular to the polarized excitation source, can be used to determine the degree of alignment (12–16). This information is important in estimating the extent of rotation of the molecule before it fragments, and affords an indirect measure of its lifetime. It is also useful for understanding the origin of rotational excitation of products. In time-resolved measurements of anisotropy in unimolecular reactions, two effects need to be considered—the loss of overall rotational coherence, and the evolution of the rotational constants and energy levels from those of the bound molecule to those of the free fragments. The simplest case is to assume that the fragmentation occurs before the molecule rotates and the distribution over product rotational states is determined instantaneously (i.e. dissociation occurs in the "Franck-Condon" region). The subsequent dynamics consists of the loss of coherence among the product states and an overall buildup of population in these states (85, 86).

The time-dependent rotational anisotropy parameter for each rotational state with angular momentum j, $r(t,j)$, defined as

$$r(t,j) = \frac{I_{\parallel}(t,j) - I_{\perp}(t,j)}{I_{\parallel}(t,j) + 2I_{\perp}(t,j)} \qquad 7.$$

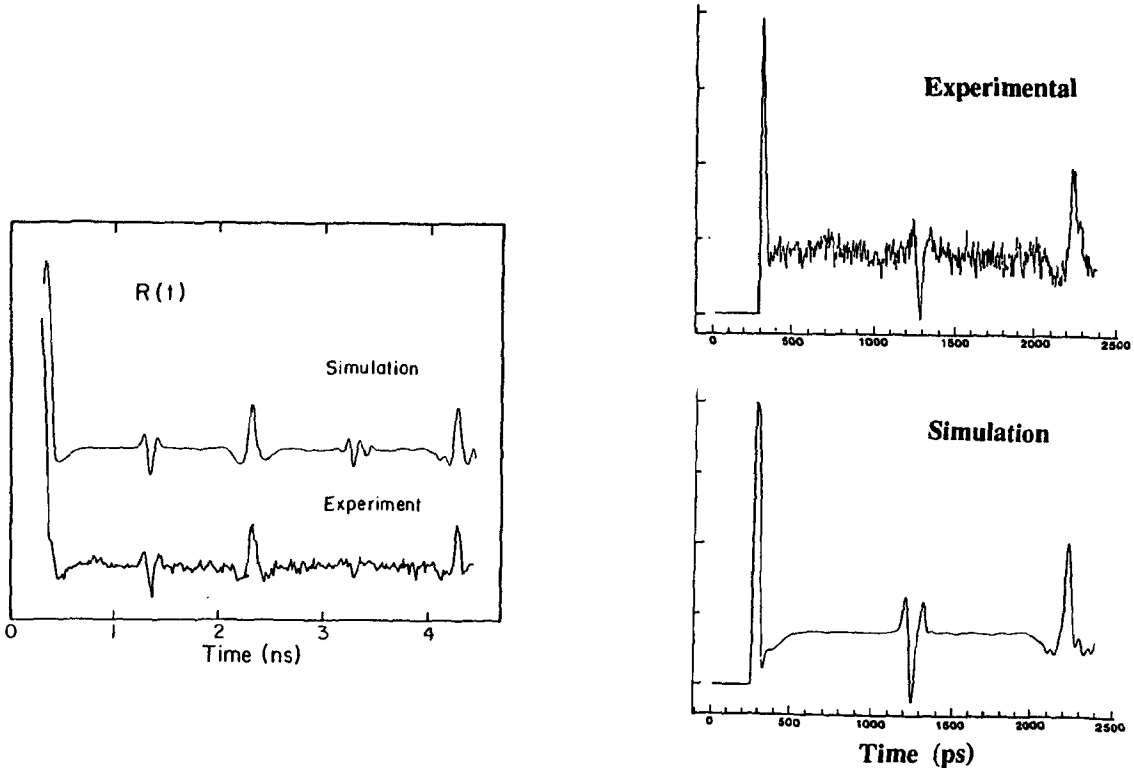

Figure 6 Rotational rephasing from the vibrationless level of stilbene S_1. The traces on the *left* show the rotational anisotropy, $R(t)$, observed in emission, with ~40 ps response function and the theoretical prediction. The set on the *right* shows the anisotropy in absorption from the excited state with better resolution (response ~10.5 ps) and the predictions for these experimental conditions. The improved resolution in the latter case allows one to see the initial loss of coherence directly (73–76, 78).

can be written in the much simpler form:

$$r(t,j) = 0.4P_2\{\cos[\eta(t)]\}. \quad 8.$$

The angle between the transition dipole moments of the states being excited by the pump laser (at $t = 0$) and that being monitored by the delayed probe pulse is $\eta(t)$. P_2 is the second-order Legendre polynomial. The observed time-dependent anisotropy, $r(t)$, is the average of Eq. 8 over the distribution of product rotational states being probed:

$$r(t) = \frac{\sum_j P(j)r(t,j)}{\sum_j P(j)}. \quad 9.$$

The averaged transient behavior observed with the polarization planes of the pump and probe pulses set parallel ($I_\parallel$) and perpendicular ($I_\perp$) to each other can be written as

$$\langle I_\parallel \rangle = \langle [1+2r(t,j)]A(t,j) \rangle \quad 10a.$$

$$\langle I_\perp \rangle = \langle [1-r(t,j)]A(t,j) \rangle \quad 10b.$$

where $A(t,j)$ is the normalized buildup of population in the product state with angular momentum j. If $A(t,j)$ is essentially the same for each j, these expressions can be further simplified to

$$\langle I_\parallel \rangle = \langle 1+2r(t,j) \rangle A(t) \quad 11a.$$

$$\langle I_\perp \rangle = \langle 1-r(t,j) \rangle A(t). \quad 11b.$$

Numerical simulations show that $r(t)$ is strongly dependent on both the average j and the width of the distribution over j, with the anisotropy persisting longer for smaller average j, narrower distributions, and, of course, smaller rotational constants (slower rotations) (85, 86). Examples of early time anisotropy for the dissociation of ICN and HgI_2 are shown in Figure 7. In each case, the calculated anisotropy has been normalized to an asymptotic value determined by theory. The steady-state values for ICN are known (87–91) but have not been used here.

With the assumptions made above, the initial loss of rotational coherence should be followed at later times (period given by $2B$) by recurrences that are clearly observable in $r(t)$. Such recurrences have been seen in product fluorescence (free stilbene) in the predissociation of a stilbene-He (92) van der Waals' complex, where the time constant for dissociation is $\sim$80 ps! This suggests that even though the complexes apparently dissociate "randomly" in time, the rotational levels of the complex evolve adiabatically into those of the free stilbene, preserving the phase coherence.

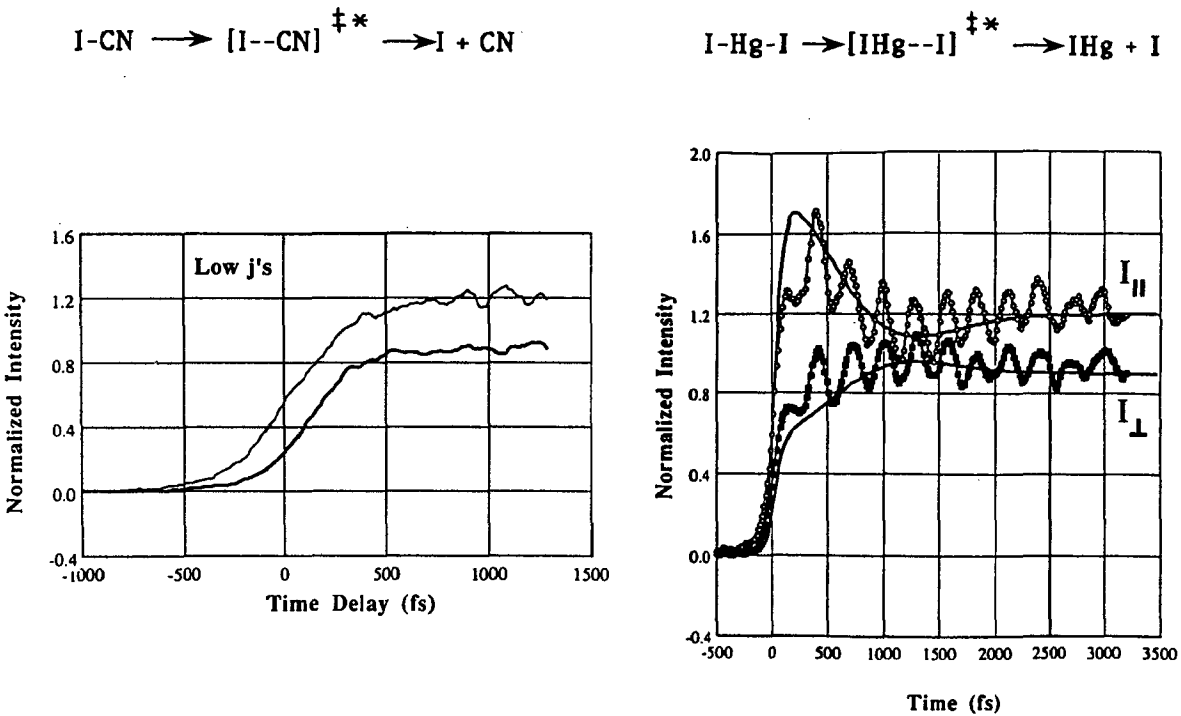

Figure 7 Femtosecond alignment for two reactions. *Left*: the ICN reaction. *Right*: similar results for the IHgI reaction. The FTS transients for HgI_2 were obtained with pump and probe polarizations being parallel (*open circles*) or perpendicular (*filled circles*) to each other. The *heavy line* through the curves is the expected signal as calculated by a simple classical method (85, 86).

This could be a result of the close similarity of the rotational constants of free stilbene ($B'+C' = 0.5132 \pm 0.0008$ GHz) and stilbene-He ($B'+C' = 0.4978 \pm 0.0019$ GHz) (76) and the fact that the rotational constants are small. As discussed in a later section, similar recurrences have also been observed when FTS is used for molecular iodine.

STATE-TO-STATE MICROCANONICAL RATES

The concept of state-to-state rates is predicated on a master equation approach to reactions. In this picture, all the energy levels of the reactant, characterized by distinct electronic (n_r), vibrational (v_r), and rotational (J_r) quantum numbers, have distinct microscopic rates for dissociation into product quantum states (n_p, v_p, J_p):

$$R(n_r, v_r, J_r) \rightarrow P(n_p, v_p, J_p)$$

The rate constants $k(n_r, v_r, J_r; n_p, v_p, J_p; b)$ may depend on the reactant and product quantum numbers, as well as some parameter, b, describing their relative motion. These ideas are applicable to both unimolecular and bimolecular reactions.

In the formulation of statistical theories of reaction rates, the microscopic rate constants are generally assumed to be proportional to the number of states, $\tilde{N}$, of the reactive system satisfying certain constraints:

$$k_s = \frac{\tilde{N}}{h_\rho}. \qquad 12.$$

The different versions of statistical theories (25–31) [RRKM and its variational modification for flexible states, phase space theory (PST), the statistical adiabatic channel model (SACM), the separate statistical ensemble (SSE)] differ in the details of the constraints assumed. We do not attempt a review of the theories here and refer the interested reader to several textbooks (93, 94), reviews (2, 3, 24, 95–97), and the original articles (25–31) on these topics.

In comparing experimental results with some theoretical model, one of course needs to know the observables of the experiment. Generally, the reagent and product states can be specified only as a distribution of the complete set of variables $\{n_r, v_r, J_r; n_p, v_p, J_p; b\}$, and the experimental rates should be compared with an average of theoretical rates over this distribution. A few simple examples will help to illustrate this point; we restrict our attention to unimolecular reactions, although the examples can be extended to include all reactions. The simplest one is that of a

thermal dissociation (or isomerization) in which the experimental variable is the temperature. The first constraint involves a particular molecular configuration with one less degree of freedom than the reactants, the so-called "transition-state." An RRKM formulation then assumes that the microscopic rate constants depend only on the available energy and total angular momentum. Averaging Eq. 12 over all possible combinations of reagent quantum states with Boltzmann statistics, one obtains the standard transition-state theory rate expression.

The most rigorous experimental tests of the rate theories will be achieved when the initial and final states are precisely specified, since then the effects of averaging are minimized. To achieve this, we have coupled supersonic beam expansions and transform-limited ultrashort laser pulses to define essentially microcanonical ensembles characterized by their energy and angular momentum. Rates measured as a function of energy provide an experimental basis for rigorous tests of statistical microcanonical rate theories. Two points pertaining to these measurements should be borne in mind. First, a simple kinetic argument shows that even if the reagent quantum numbers were uniquely determined by the excitation process, the rate constant for the loss of population in this state would be given by the sum of the microscopic rate constants connecting it to all possible product states:

$$k_{\text{obs}}(n_r, v_r, J_r) = \sum_{\{n_p, v_p, J_p; b\}} k(n_r, v_r, J_r; n_p, v_p, J_p; b). \qquad 13.$$

In this idealized case, the decay of the initial state and the buildup of population in *any* of the product states is purely single exponential, with the same time constant, k_{obs}^{-1}. Within the limits of this master equation-like approach, the state-to-state rate constant can be obtained as the product of the asymptotic, relative probability of forming products with a particular combination of quantum numbers and this rate constant, k_{obs}.

Inasmuch as the experimental conditions only specify the energy level and not the individual quantum states, the temporal behavior of the initial state, $S_r(t)$, is a sum of single exponential transients weighted by the probabilities of creating and detecting each $\{n_r, v_r, J_r\}$:

$$S_r(t) = \sum_{\{n_r, v_r, J_r\}} P^{\text{ex}}(n_r, v_r, J_r) P^{\text{det}}(n_r, v_r, J_r) \cdot \exp[-k_{\text{obs}}(n_r, v_r, J_r)t]. \qquad 14.$$

The corresponding expression for the signal when a product state is being monitored is also a sum, with $P^{\text{det}}(n_r, v_r, J_r)$ being replaced by the probability for detecting the final state and the exponential decay replaced by

a kinetically weighted buildup term:

$$S_p(t) = \sum_{\{n_r,v_r,J_r\}} P^{ex}P^{det}(n_p, v_p, J_p)\frac{\sum_b k(n_r, v_r, J_r; n_p, v_p, J_p; b)}{k_{obs}}\cdot[1-e^{-k_{obs}t}]. \quad 15.$$

For a purely microcanonical initial state, i.e. a system whose energy and angular momentum are uniquely determined, a statistical reaction will result in identical temporal evolution in all product channels and a random distribution of survival probabilities (98) (single exponential decays). If a single molecular eigenstate is excited, one will also see the same behavior. Restrictions in phase space or incomplete (in a spatial sense) redistribution may result in nonexponential behavior, depending on how the system is prepared. For example, consider the case where the reagent phase space is divided into two noncommunicating parts, A_1 and A_2, the first leading to product B_1 only and A_2 yielding a different product quantum state B_2 only. If the exponential rate constants from A_1 and A_2 are substantially different, the population of reactants (A_1+A_2) will show a biexponential decay, while B_1 and B_2 will show exponential buildup with different characteristic constants. Finally, it should be emphasized that if a coherent preparation of eigenstates is made, then an initial rapid redistribution (dephasing) followed by the decay of eigenstates will be observed.

As a concrete, illustrative example we discuss the photodissociation of nitrosyl cyanide (NCNO) into the diatomic radicals NO and CN:

$$NCNO \rightarrow CN + NO.$$

This molecule has a low-lying excited singlet electronic state that is heavily mixed, presumably with the ground state, as evidenced by the excitation and fluorescence spectra. In a series of state-of-the-art experiments, Wittig and Reisler have obtained the complete nascent internal state distribution of the products of the visible photolysis of the weak (17085 cm^{-1}) central C–N bond were measured for excess energies up to 5000 cm^{-1} above threshold (99–102). The rotational state distributions for both CN and NO were found to be almost exactly as predicted by phase space theory (PST). The observed relative populations in the two spin-orbit states of NO were found to be different from expectations based on PST; recent correlated Doppler spectroscopy of the fragments suggests that a plane of symmetry may be preserved during dissociation.

We have measured (103) rates of dissociation near threshold (5–600 cm^{-1}) from jet-cooled NCNO (Figure 8) and found them to increase generally with excess energy. Product buildup in different rotational states of the CN fragment for a fixed excitation energy was independent of the character of the final state if the initial state was internally cold. The

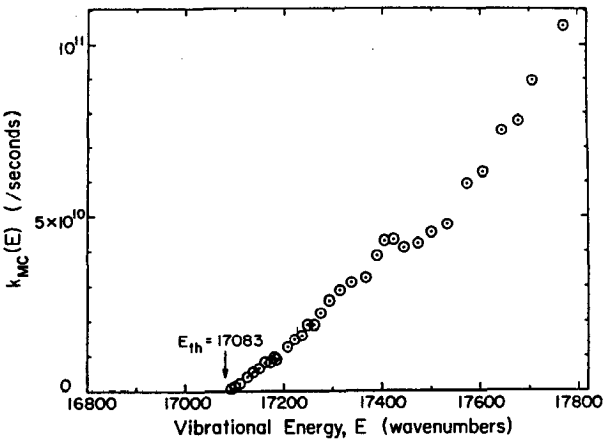

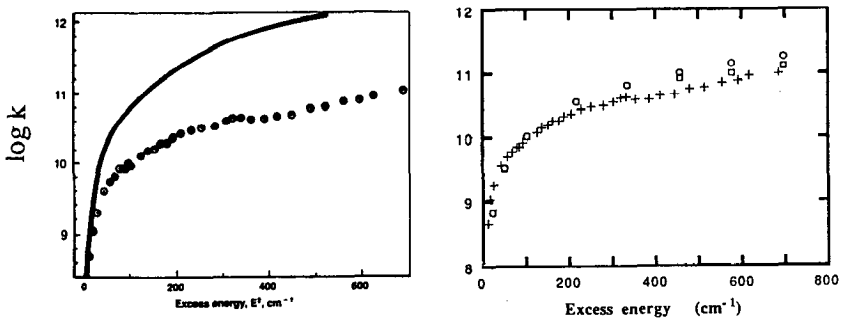

Figure 8 Microcanonical state-to-state rates for the reaction of NCNO. The *upper panel* shows the rates as a function of energy. In the *lower panel* (*right*), logarithms of the experimental rates (+) are compared with variational RRKM calculations for two different surfaces (*squares* and *open circles*). The *lower left* is a comparison of experiments with quantum PST calculations that show the large discrepancy above threshold. Note the features in $k_{MC}(E)$ (see text and 103, 107).

exponential time-constant for loss of NCNO, measured by using a UV photon to promote the dissociating system to a higher electronic state that formed electronically excited CN fragments, was identical to the lifetime measured in the buildup of fragments. This has helped us to separate the dynamics in terms of IVR and bond-breakage. The barrier to dissociation on the triplet surface (104, 105) has been calculated to be much higher than the energies considered here. Accordingly, the triplet state is assumed to play a minor role.

The excess energy dependence of the rates shows large deviations from Phase Space Theory, particularly for energies significantly higher than threshold. It also shows some unusual features: a change to smaller increases with energy in the range of 200–350 cm^{-1}, and a weak local maximum at ~ 320 cm^{-1}. The trends of $k(E)$ vs E cannot be explained quantitatively by PST, which was used successfully to model the product state distributions at these energies. The variational RRKM method can be used to get results that are in better agreement with our experimental rates (107). In contrast to a quantum PST calculation, the variational RRKM (and the classical PST) calculations circumvent the problem of determining the proper electronic degeneracy by the choice of the adiabatic potential surface on which the reaction occurs. The results suggest the change in the position of the effective transition-state along the reaction coordinate as a function of energy. The importance of rotations on reaction rates has been shown by Troe (106), but SACM has not been applied to this reaction yet.

The differences between trends in the measured and calculated rates could be the result of a poor choice of the potential energy surface. The features in the excess energy dependence mentioned above, however, may suggest the possibility of incomplete energy redistribution in NCNO at these energies. Other indications that these subtleties may be signatures of the coherent excitation process or dynamics of energy flow include sharp, well-defined resonance absorption features in the photofragment yield spectrum and the nonstatistical distribution of products in the different spin-orbit states of NO.

Overtone-initiated dissociation in a collisionless gas (108–115) provides a case in which the effects of vibrational redistribution on dissociation rates can be studied on the ground electronic surface. Rates estimated from linewidth studies on peroxides and product state distributions (PSD) have been compared favorably with calculations (111–115) based on the SACM theory by Troe and Crim. Direct time-resolved measurements on the dissociation of hydrogen peroxide (116)

$$HOOH(v_{OH} = 5) \rightarrow HO + OH$$

in a bulb at room temperature showed nonexponential buildup of fragments and a strong dependence on the excess energy and the fragment rotational state being monitored. The observed trends could be qualitatively explained by rates estimated from PST and a distribution of energies and angular momenta in the ensemble; this underscores the need for measuring microcanonical rates for testing rate theories. The width corresponding to these measured rates has no relationship to the apparent

spectral bandwidth, which was shown to be inhomogeneously broadened (111–116).

Product state distributions for the near UV photolysis of ketene (117, 118)

$$H_2C = C = O \rightarrow CH_2 + CO$$

have also been found to be consistent with PST. Microcanonical rates for this reaction have been measured (119) over a much larger range of excess energies than the previous example of NCNO (Figure 9). In this case as well, PST greatly overestimates rates; the variational RRKM theory calculations (120) (assuming a potential surface) show a dramatic improvement over the PST model and are in good agreement with the overall trend of experimental results. No SACM calculations are available yet.

In the UV (266–308 nm) photolysis of 1,2-diiodotetrafluoroethane, a sequential bond fission mechanism was identified (121, 122):

$$C_2F_4I_2 \rightarrow C_2F_4I + I(^2P_{1/2}, {}^2P_{3/2}) \quad \text{(primary)}$$

$$C_2F_4I \rightarrow C_2F_4 + I(^2P_{3/2}) \quad \text{(secondary)}$$

In the first step, I atoms are formed in a very short time (< 1 ps), and the radical C_2F_4I is formed with enough internal energy to dissociate spontaneously. For high photolysis energies (266 nm), I atoms are formed predominantly in the excited spin-orbit state whereas only ground state I atoms are formed in the second step. The buildups in the two different product channels are drastically different (Figure 10). This second step

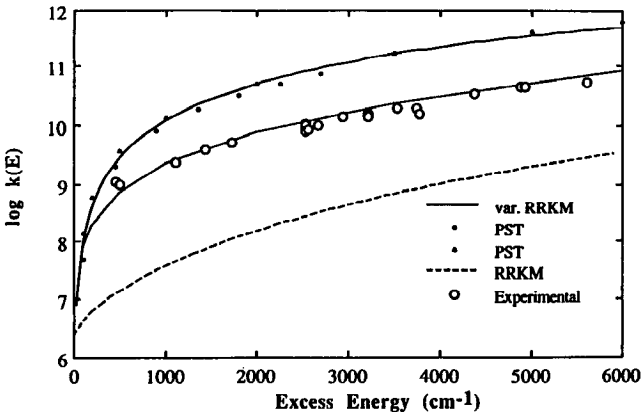

Figure 9 Microcanonical state-to-state rates as a function of excess energy in the reaction of ketene to carbon monoxide and methylene. The variational RRKM treatment agrees well with the data, in contrast to standard RRKM or PST rates (see text and 119, 120).

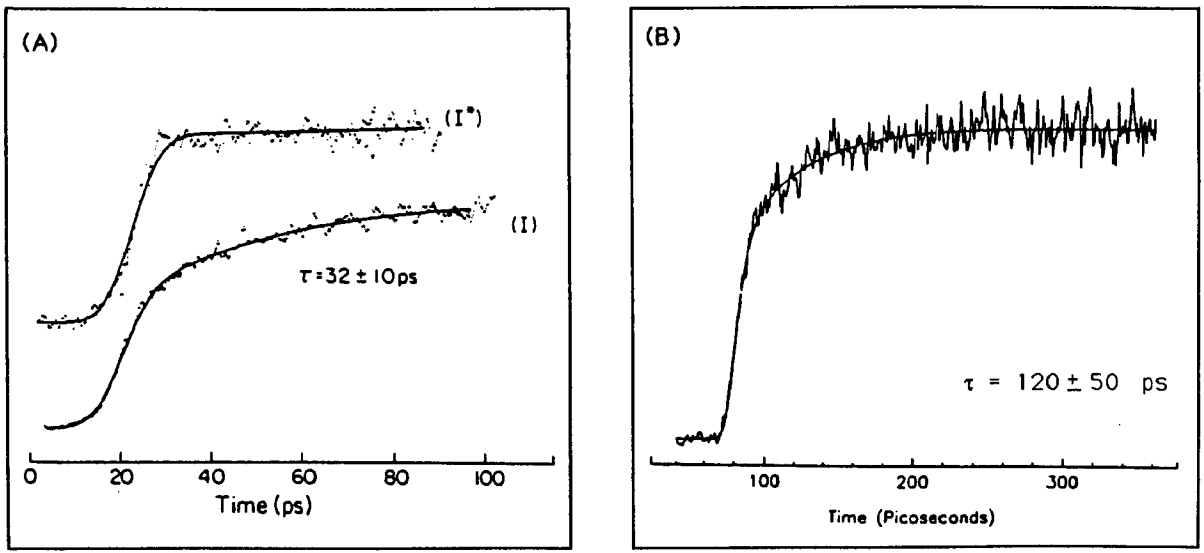

Figure 10 Stepwise bond breakage in the reaction of I–CF_2–CF_2–I. The figure shows the differences in product buildup in the two lowest spin-orbit states of I atoms. The first step producing predominantly I* is prompt (< 1 ps), and the second step producing ground state I is slow (~30–120 ps), depending on the internal energy of the radical. Some ground state I atoms are formed promptly when the photolysis wavelength is significantly redder than 266 nm (see 121, 122).

shows a biexponential buildup due to the distribution of internal energies resulting from the first step. The slow component changes from ~30 ps to ~120 ps when the photolysis wavelength is increased, a result of less energy being channeled into radical internal states.

In this group, several other reactions have been studied: phenol- and *p*-cresol-benzene complexes (123), stilbene-He(Ne, Ar) complexes (124, 125), isomerization of *trans*-stilbene (126), proton transfer studies in methyl salicylate (127), and intramolecular charge transfer reactions (128). Other groups have also studied the predissociation of tetrazine-Ar in both the excited state (129) and the ground state (130), and dimers of NO in the ground state (131). The topic of predissociation dynamics as obtained from high resolution studies has been reviewed recently (132, 133) and is not covered here.

FTS AND TRANSITION-STATE DYNAMICS IN REAL-TIME

The precise shape of the multidimensional potential energy surface is critical to our understanding of chemical reaction dynamics. Until recently, direct spectroscopic studies were used to explore only a small region around the stable configurations but not including transitory species—transition state species—that correspond to nonequilibrium configurations that are neither reactants nor products. The unique "critical complex" of transition state, activated complex, or absolute rate theory, is one of many such nonequilibrium configurations. Major efforts have been focused on advancing transition-state spectroscopy (for reviews see 32–34). Emission, scattering, absorption, CARS, and electron photodetachment methods have been developed to probe nonequilibrium regions of potential energy surfaces (134–139).

In recent years, it has become possible to study the dynamics of transition states in real-time by using femtosecond transition-state spectroscopy (FTS) (32–34, 140–144). The duration of the pulses is generally shorter than the "lifetime" of the transition states, and this allows one to monitor the evolution from reagents to products with $\sim 10^6$-fold greater sensitivity. The concepts involved in FTS have been discussed elsewhere (32–34, 140–144), and the idea is simple. Long-lived products have narrow spectroscopic linewidths, and in measuring the buildup of population in product states spectroscopically, one would normally tune the frequency of the laser to the peak of a resonance in its absorption spectrum. The observed temporal behavior is a monotonic increase in signal. If the laser is tuned off-resonance, those transition-state species whose energy levels are perturbed relative to the products such that their transition energy is now resonant

with the probe frequency, will be preferentially excited. The temporal behavior in this case will exhibit an initial increase in signal, followed by a drop and ultimate leveling-off at some value lower than the maximum. The ratio of the amplitude at very long time to the maximum signal depends on the amount of detuning. Thus, these transients bear the signature of the interaction potential and provide a means of selectively observing perturbed products or transition-state species. Basically, the ultrashort pulse "opens" a window on the potential surface and the FTS data can be inverted to deduce the potential as prescribed in (145) for simple reactions.

A simple classical description of FTS applied to bond fission has been given (146). For illustration, we consider a pair of one-dimensional potential energy curves, one on which the initially prepared state evolves and the other that of an electronic excited state of one of the products which is being monitored (Figure 11). The evolution is simply the classical motion of particle (reduced mass m) on potential V_1. If E is the initial energy, R_0 is the position at zero time and $V_1(R_0) = E$, then by elementary Newtonian mechanics:

$$R(t) = R_0 + \int_0^t \left[\frac{2}{m}\{E - V_1(R(\tau))\}\right]^{1/2} d\tau. \qquad 16.$$

The energy of the optical transition at time t is given by $V_2[R(t)] - V_1[R(t)]$. These equations can be analytically solved for some cases such as: (*a*) when $V_1(R)$ is an exponential function of R and (*b*) when it is an inverse square function of R. The exact form of the observed transient behavior will depend on the extent of detuning (i.e. probe wavelength), its spectral width, and of course the intrinsic molecular dynamics. Some typical results are shown in Figure 12.

For the case of a repulsive potential, the system continues to move indefinitely. Since the transition from reactants to products is continuous and does not occur randomly in time, a reaction rate constant cannot be defined. On the other hand, a phenomenological reaction time, τ_d, analogous in spirit to the concept of time-delay in scattering studies, can be defined. Because the pulse opens a window of finite width on the PES, the exact definition of bond-breaking time can be related to this window and characteristic of the PES; this is discussed in greater detail in Refs. (140–146). From a practical point of view, the bond may be considered broken when the window no longer distinguishes between transition-states and free products, within the limit of the uncertainty principle.

We illustrate these concepts with two examples, one involving the direct breakage of a bond (repulsive PES) and the other involving a nonadiabatic dissociation due to the avoided crossing of covalent and ionic potential

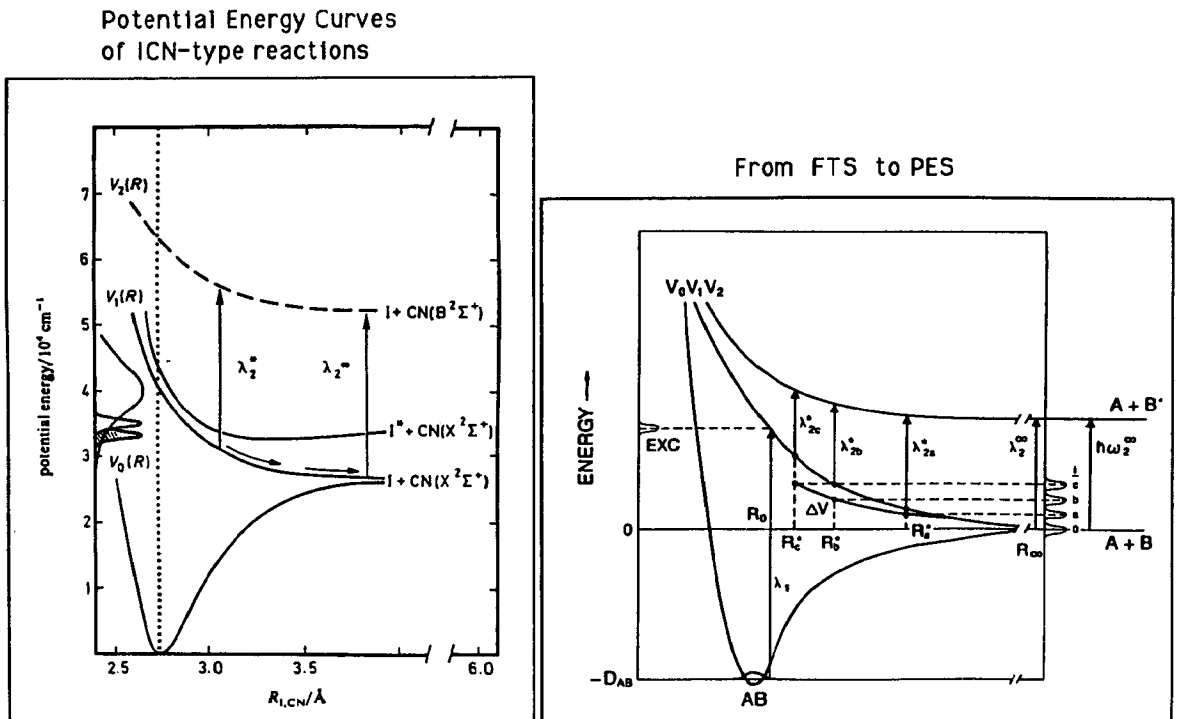

Figure 11 Concept of FTS illustrated on ICN reaction surfaces (figure on *left* from Ref. 143). The figure on the *right* shows how the probe "opens a window" of detection on the PES (from Ref. 145).

curves. Figure 12 shows experimental transients (140–144) obtained with different probe wavelengths for the dissociation of ICN:

$$ICN \rightarrow [I \cdots CN]^{\ddagger *} \rightarrow CN + I(^2P_{3/2}).$$

Although both spin-orbit states of I are known to be formed in this reaction, the photolysis energy in these FTS experiments is not sufficient for dissociation into the spin-orbit excited ($^2P_{1/2}$) channel. The measurement of the system response function is an important part of the experiment, since pulse broadening in transmission through dispersive media can be a major source of error in pump-probe transients with ultrashort pulses. In addition, one can determine the initial time ($t = 0$) accurately. This measurement was made by monitoring the photo-ion current obtained from the [1 + 1] UV photoionization of a standard compound (*N*, *N*-diethylaniline) in situ.

The classical mechanical model of the dynamics describes the results fairly well (142, 143, 146). Quantum calculations using Heller's wave-packet method (147) have been performed by Williams & Imre (148); trajectory calculations by Benjamin & Wilson have also been reported (149). They are both in agreement with experimental results. The effect of rotations was considered by Metiu's (150) and by Heller's groups (151) and by one of us (85). Mukamel (152) has formally shown the effects of quantum coherence and dephasing, and his results are also in accord with experiments. Shapiro & Bersohn have considered the problem using the frequency domain approach (153). For a related problem, Kono & Fujimura (154) have treated wave packet dynamics and Yamashita & Morokuma (155) have computed trajectories on dressed PES, with an interesting new focus.

In the dissociation of sodium iodide (156–158), direct observation of photofragment trapping resonances were made:

$$NaI \rightarrow [Na \cdots I]^{\ddagger *} \rightarrow Na + I.$$

When the probe is resonant with "free" Na atomic transitions, the buildup consists of a periodic sequence of step functions; when it is tuned off-resonance, an oscillatory signal is seen (Figure 13). The period of these oscillations reflects the nature of the potential that has been studied by other methods (see 156 for details). In this system, there are covalent and ionic surfaces that cross at ~ 7 Å. The covalent surface leads to free atoms and the other leads to ionic products. The observed resonances are the quantum states of the heavily distorted, mixed ionic and covalent potential well. The decay of the initial state and the buildup of free products in ~ 10 ps yields the interaction (coupling strength) between the two surfaces (156–158). Note also that the formation of products is not random in time, as

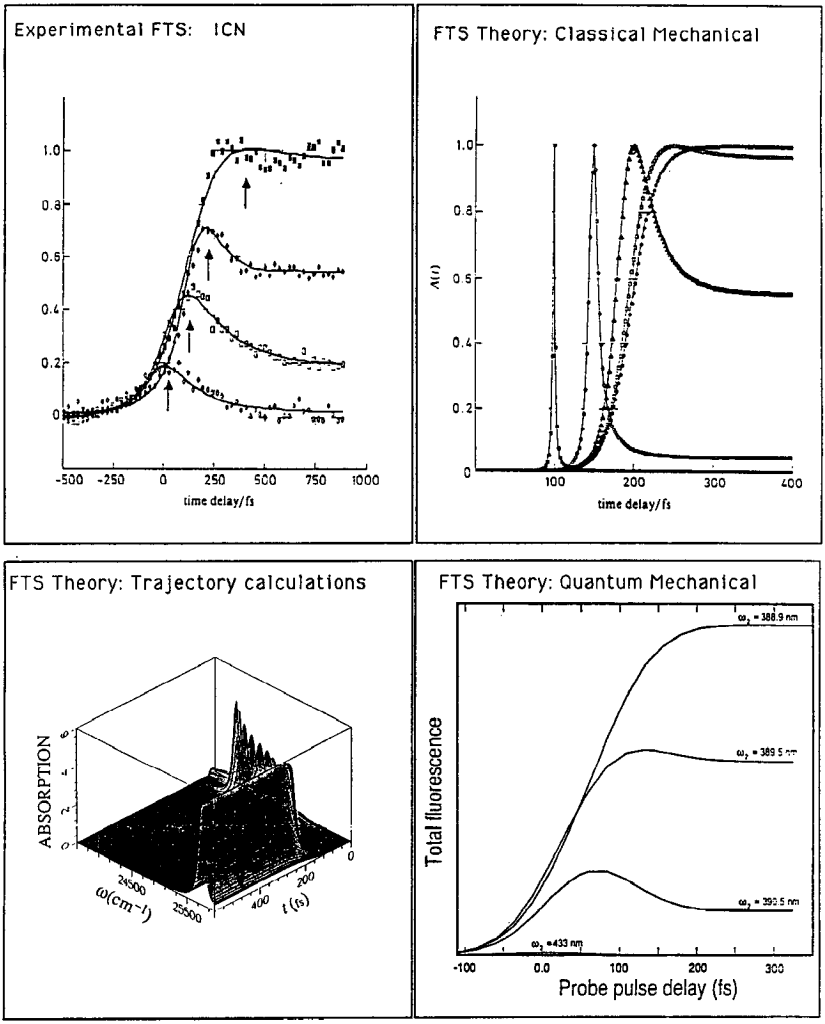

Figure 12 Experimental and theoretical FTS results on ICN reaction. *Top left*: transient behavior observed in the dissociation of ICN by the FTS method at different probe wavelengths (see Fig. 11 and Ref. 143). *Top right*: the predicted transient behavior from the classical model for the dissociation of ICN (142, 143). *Bottom left*: time-dependent spectrum from trajectory calculations (149). *Bottom right*: the results of a quantum simulation (148). All calculations are in agreement with experiments.

should be the case if a kinetic scheme were appropriate for this reaction, and the effects last tens of picoseconds, i.e. the system exhibits resonance effects! Detailed studies of these alkali halide reactions have allowed us further to characterize the dynamics in terms of the dephasing of wavepackets, the Landau-Zener escape probability, and the period of wavepacket motion. The period of recurrences varies with the excitation energy and has been related to the anharmonic interatomic potential. These results therefore provide a direct view of the evolution of the quantum wavefunction and the potential energy (ionic/covalent) for fragment separation. In these prototype systems, classical and semiclassical (156–161), and quantum (162–165) calculations have all reproduced the major features of the FTS experiments.

FTS of iodine (I_2) (166–168) has also shown that vibrational and rotational motion can be observed in real-time (Figure 14). The period of the observed vibrational oscillations and the recurrences observed on a longer timescale due to rotations have been inverted to obtain accurate potential energy curves (168). When the system is excited to a dissociative surface, features similar to those presented earlier for ICN are seen:

$$I_2 \rightarrow [I \cdots I]^{\ddagger *} \rightarrow I + I \qquad (a)$$

$$I_2 \rightarrow [I \cdots I]^{\ddagger *} \rightarrow I_2 \qquad (b)$$

FTS studies have been recently extended (169, 170) to treat systems with more than one degree-of-freedom:

$$HgI_2 \rightarrow [IHg \cdots I]^{\ddagger *} \rightarrow HgI + I \qquad (a)$$

$$HgI_2 \rightarrow [I \cdots Hg \cdots I]^{\ddagger *} \rightarrow Hg + I + I \qquad (b)$$

In this system, the vibrational motion of the HgI fragment participates directly in the dissociation process and the PES has a well-defined saddle point—the symmetric coordinate is "bound" and the antisymmetric one is repulsive (see Figure 15). As before, the pump pulse initiates the reaction and the probe pulse excites a distribution of vibrational states of the HgI fragment to a fluorescent, excited electronic state. The emission from this state can be spectrally resolved and used to deduce the nascent distribution of HgI vibrational states. With a narrow spectral window and both pump and probe frequencies fixed, the evolution of population in these vibrational states can be monitored in real-time. The I–Hg–I bending motion evolves into rotations of the HgI fragment and measurements of the time-dependent anisotropy (see section on *Polarized Photofragment Spectroscopy*, above) provides a means of monitoring this degree of freedom as well (85, 86, 169, 170). Typical results are shown in Figure 7. Detailed classical and semiclassical calculations of FTS are in good agree-

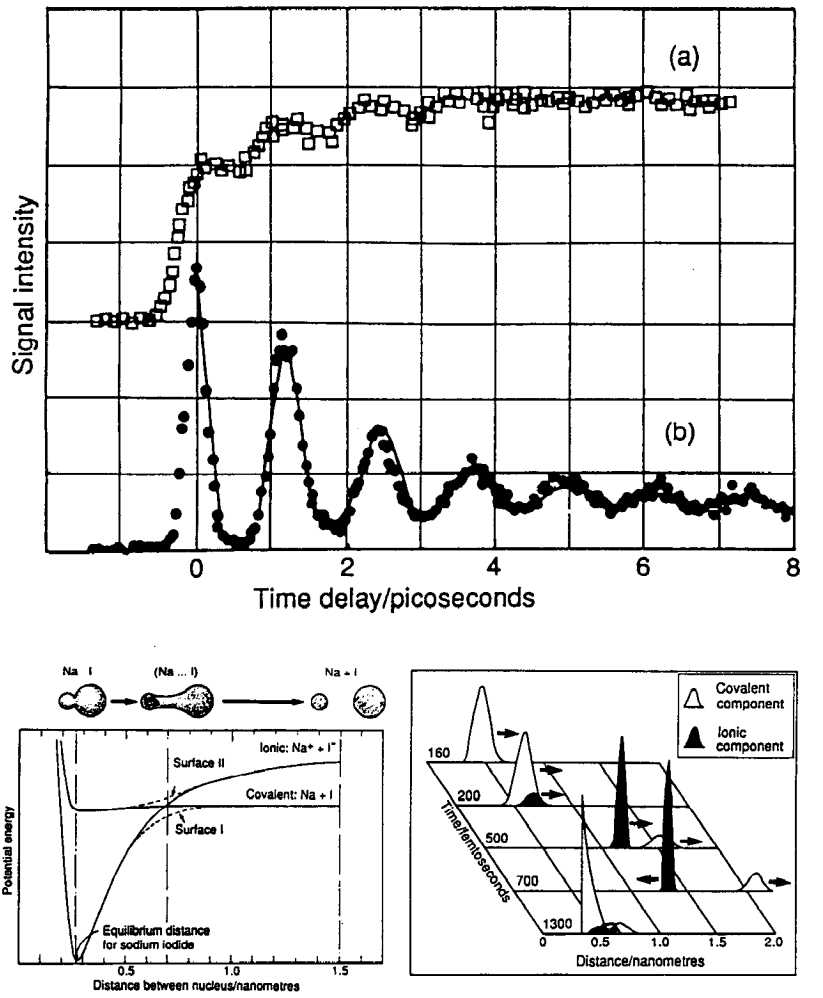

Figure 13 (*Top*) FTS of sodium iodide showing the photofragment trapping resonance. The phenomenon can be visualized as the motion of a wavepacket in an anharmonic well formed by the avoided crossing between the covalent and ionic surfaces (*lower left*), with a small probability of forming products during each period of its motion. Results of quantum calculations (*lower right*) show how the initial wavepacket splits into two parts—ionic and covalent—each time it passes through the crossing region (see 156–158, 162, 32, 200).

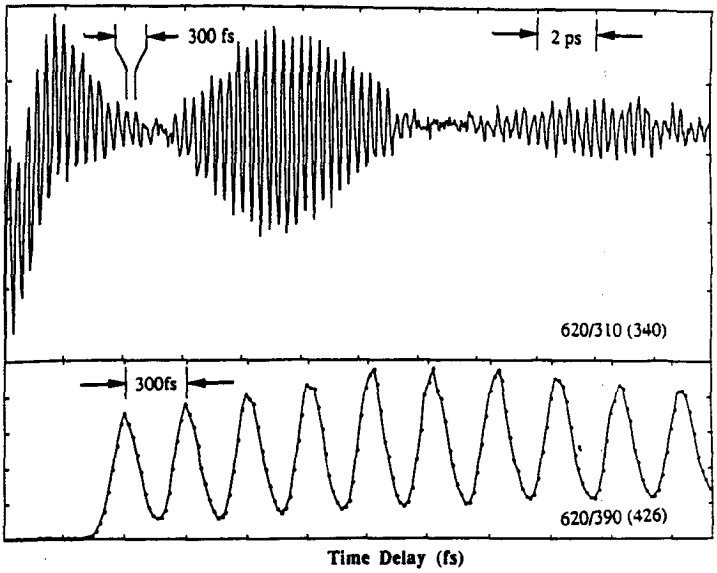

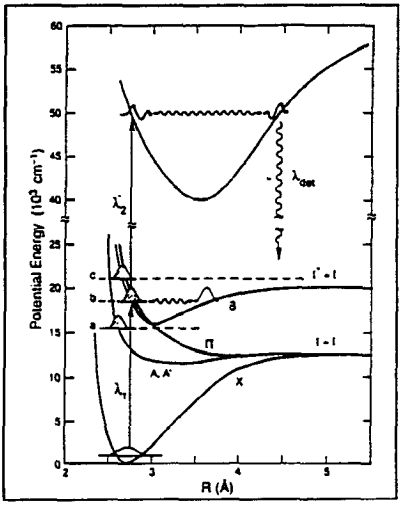

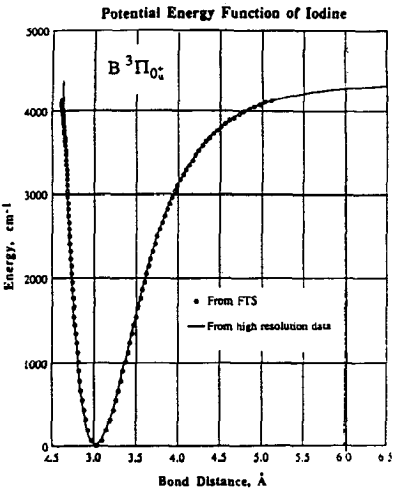

Figure 14 (*Top*) FTS transients of molecular I_2: a long (time) scan showing constructive and destructive interferences between the different states in the wavepacket. The pump wavelength was 620 nm, the probe wavelength 310 nm and emission at 340 nm was detected. The high frequency oscillation corresponds to the period of the wavepacket. The second trace (shorter time range) shows the effect of changing the probe wavelength to 390 nm and detecting at 426 nm. *Bottom* (*left*): the various schemes for FTS detection; (*right*) the deduced PES from inversion of FTS data. Note the excellent agreement between these results (*solid circles*) and the known PES (for details see 168).

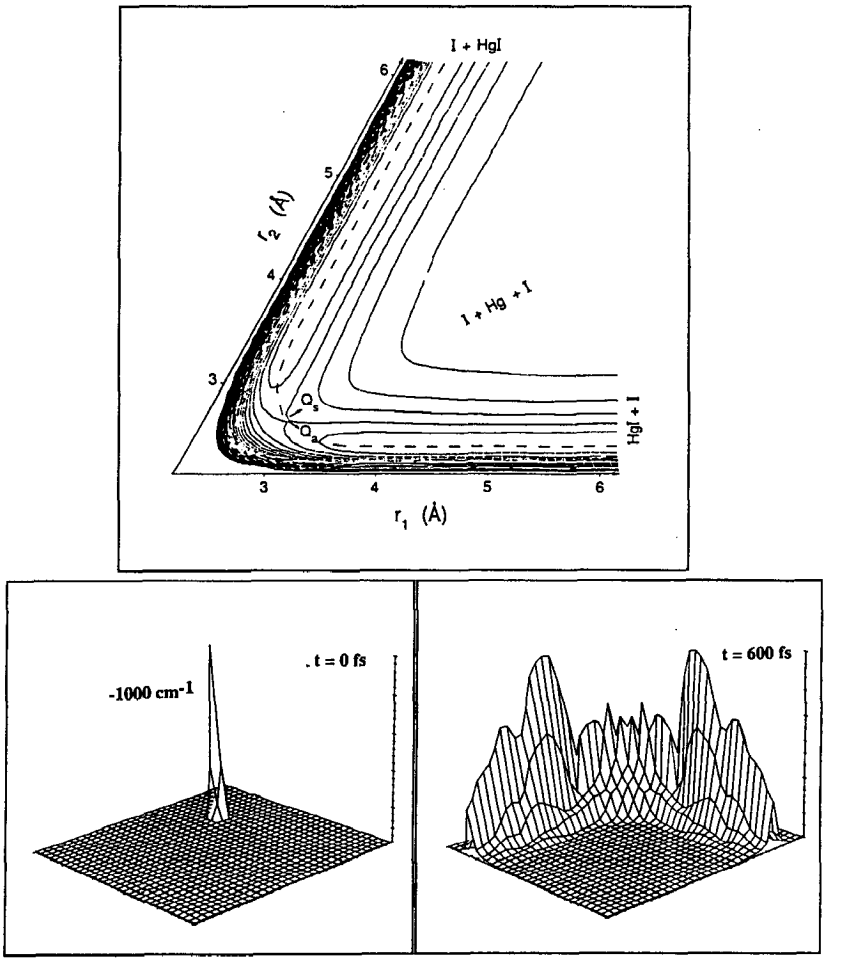

Figure 15 The PES and wavepacket motion for the reaction of IHgI on the excited surface. FTS transients are shown in Figure 7. The *upper figure* shows contours of the potential energy as a function of the symmetric and antisymmetric stretching coordinates (169, 170). The *lower figure* shows a quantum calculation of a wavepacket at 0 fs and at 600 fs for this reaction. The latter indicates how the fragments separate into products in the HgI+I channels. The available energy in these simulations was 1000 cm^{-1} below dissociation into Hg+2I. Recent calculations have provided both the PSD and FTS of the reaction (M. Gruebele, G. Roberts, A. H. Zewail, *Philos. Trans. R. Soc.* London, *Ser. A*, in press).

ment with experimental results (169, 170). Quantum calculations in 2-D have also been performed in this laboratory (Gruebele et al; see Figure 15) and agreement with experiments has been used to deduce details of the dynamics on the PES.

Other systems under consideration are methyl iodide (171, 172) and hydrogen peroxide (173):

$$CH_3I \rightarrow [CH_3 \cdots I]^{\ddagger *} \rightarrow CH_3 + I$$

$$HOOH \rightarrow [HO \cdots OH]^{\ddagger *} \rightarrow OH + OH$$

Preliminary studies were made with picosecond pulses and yielded the expected results depending on detuning. FTS studies are underway.

REAL-TIME CLOCKING OF BIMOLECULAR REACTIONS

In a photoinitiated unimolecular reaction, half-collision, the initial time is precisely defined by the excitation pulse. An equivalent initial time for a bimolecular reaction is the instant the two reactant species "find each other." Although this is conceptually simple, its experimental determination is somewhat complicated. Simply using a laser to photodissociate a precursor for one of the reactants is not sufficient, since the delay between initiation and an encounter is random and can be very long (nanoseconds to microseconds), depending on the concentration (partial pressure) of the reactants.

One class of reactive molecular systems offers a rather unique opportunity to define initial time more precisely. In these systems, the precursor and one of the reactants are prepared in a weakly bound complex. Now, the reactive group of atoms is held close together and the reaction—the so-called "vdW impacted bimolecular reaction"—can be initiated by a pulse that photolyzes the precursor. This also defines the initiation of the reaction. If the reaction is direct, i.e. potential scattering without resonances, the buildup of products should show delay times as in the previous case of half collisions. When intermediates are observed, the buildup and decay should be a function of the lifetime of the intermediate. As pointed out elsewhere (85), the vector properties of the reaction can also be identified if polarized pulses are used.

An added advantage to studying dynamics in such a "precursor complex" is that the reactants are arranged in a restricted range of possible geometries, thus the range of impact parameters is limited. However, the amplitude of the intermolecular vibration is large and the impact parameters are not really narrowly restricted. For product state distributions, such studies were pioneered by Soep and coworkers (174, 175) and by Wittig and coworkers (176, 177). The Wittig group has shown that the OH rotational distributions from the hot atom reaction initiated by the photolysis of HBr in the $BrH \cdots OCO$ complex were found to be colder

than the distributions obtained for the same reaction in a bulk gas (178–184). The HOCO molecule is known to be bound from matrix isolation studies (185, 186) and can exist in either a *cis* or a *trans* geometry (187). It has been postulated as an intermediate in the hot atom reaction (Figure 16) and has also been invoked in the interpretation of kinetic data obtained by Smith (188–190), by Golden (191), and by Benson (192). In the PES and trajectory calculations of Harding and Schatz (193, 194).

The real-time measurements (195, 196) of the buildup of free OH radicals from this reaction

$$H + CO_2 \rightarrow [HOCO]^{\ddagger *} \rightarrow CO + OH$$

initiated in the IH $\cdots$ OCO precurser indicate that the reaction is of the complex-mode type and the lifetime is relatively long, ~ 5 ps (Figure 16). A simple interpretation of the rate of OH formation as the rate of HOCO decomposition overlooks the dynamics of formation of the intermediate; the timescale of the formation reaction appears to be on the order of ~ 1 ps, close to the resolution for these initial experiments. Since there are two channels for the dissociation of HI associated with the two lowest spin-orbit states of a free I atom, the kinetic energy distribution of H atoms is likely to be bimodal, and hence two energies are available for the hot atom reaction for each photolysis wavelength. The effects of these two channels may be manifested in a variation of the buildup time among different product states, as has been observed in these experiments (195, 196). In the future, FTS experiments should reveal the passage through the transition-state as in the half-collision studies. A great deal of work in this area is underway, as we now can study a whole class of bimolecular reactions with the zero-of-time precisely defined.

A new study for a different class of bimolecular reactions has just been initiated in this group. These are intracluster reactions in which, for example, a hydrogen atom is transferred to another molecule in the cluster. For the case of α-naphthol-$(NH_3)_n$, there is no proton transfer until $n \geq 3$ (Figure 17). In clusters of water instead of ammonia, there is no proton transfer from naphthol up to 20 water molecules (197). These studies are for neutral species. Recent work on $I_2^-(CO)_n$ clusters in the Lineberger group (198) has shown that such "ion-molecule" reactions can be studied in real-time.

CONCLUDING REMARKS

Over the last decade, ultrafast (femtosecond to picosecond) dynamics in real-time has been developed and applied in a number of areas. This review has focused on three of the major areas: (*a*) vibrational and rotational

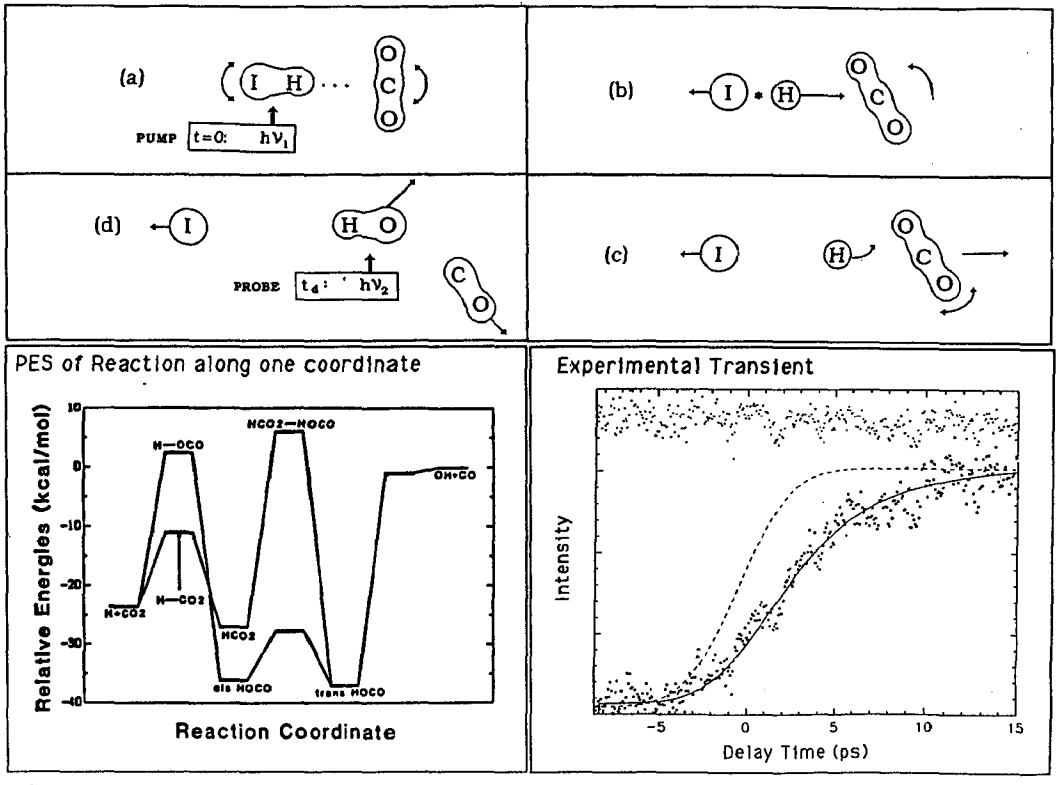

Figure 16 Bimolecular reactions in real-time. Schematic of hot atom reactions initiated in a vdW precursor complex (*top*) (196). The *lower left panel* shows the relevant energetics for the reaction of H with CO_2 (193, 194). *Lower right*: transient behavior in the buildup of OH radicals in the bimolecular reaction. The *circles* denote the data, the *dashes* represent the response function determined in situ, and the *solid line* a best fit to a kinetic model for the reaction involving HOCO as an intermediate (196).

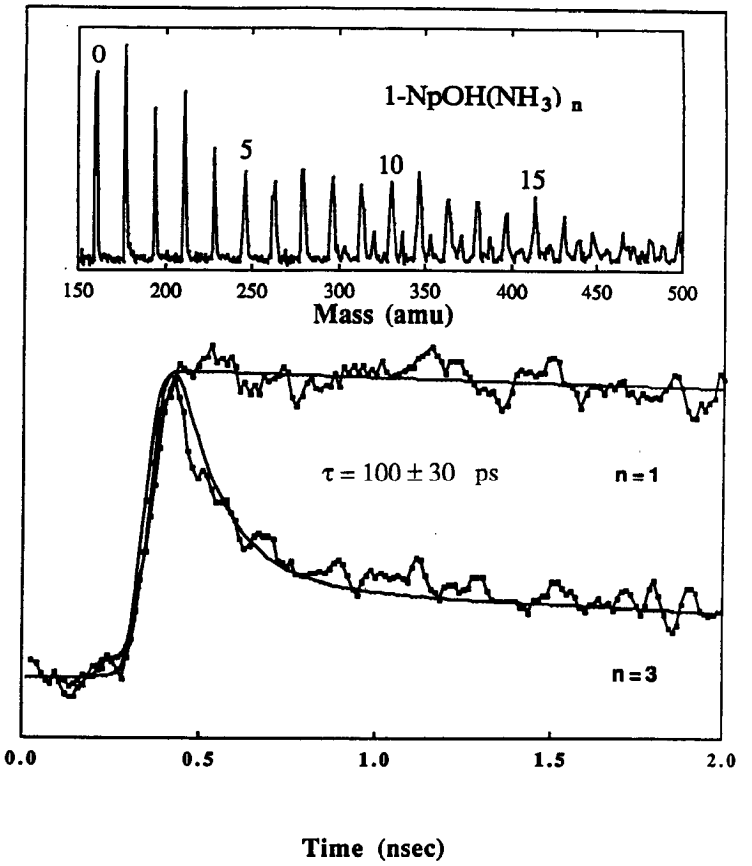

Figure 17 Bimolecular reactions in a cluster: proton transfer in 1-naphthol-$(NH_3)_n$ as a function of cluster size. The *insert* is a mass spectrum showing clusters of different sizes. The difference between the transients for $n = 1$ and $n = 3$ is due to proton transfer in the larger cluster (see 197).

energy redistribution in polyatomics; (*b*) state-to-state dynamics of uni- and bi-molecular reactions; and (*c*) direct observations of transition states. Figure 18 shows the progress made and the systems studied so far.

Picosecond energy flow—vibrational-energy redistribution (IVR)—has now been observed in many molecules. Basically, three regions, depending on energy, have been identified: no IVR, restricted IVR, and dissipative IVR. Each region has a direct signature in real-time measurements, ranging from the observation of vibrational quantum beats (in-phase and out-of-phase) between few levels (at a total vibrational state density of 200–1000

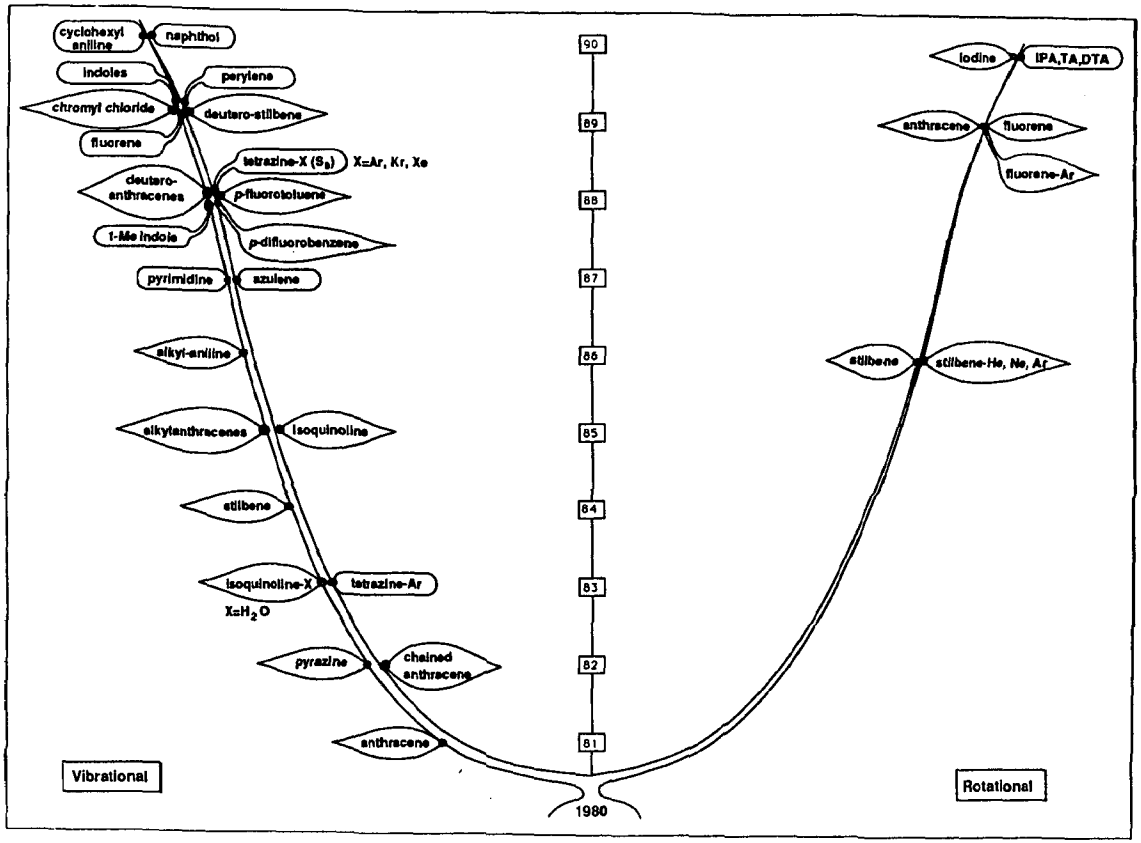

Figure 18a

Figure 18 Time-ordered "tree" for ultrafast molecular reaction dynamics showing the progress and systems studied so far: (*a*) picosecond energy flow dynamics involving vibrational and rotational redistribution; (*b*) picosecond reaction dynamics and microcanonical rates; (*c*) (p. 54) femtosecond reaction dynamics and detection of "transition-states." The *spade-shaped leaves* represent work done in this laboratory (the *dotted* ones are for work in progress). The *smoothed rectangular* ones represent work done by other groups involved in this area of research. See text for all references except the following: (*a*) cyclo-hexyl aniline (203), IPA, TA, and DTA molecules (204); (*b*) DPB (205), styrene (206), isoquinoline-X (207), aniline-

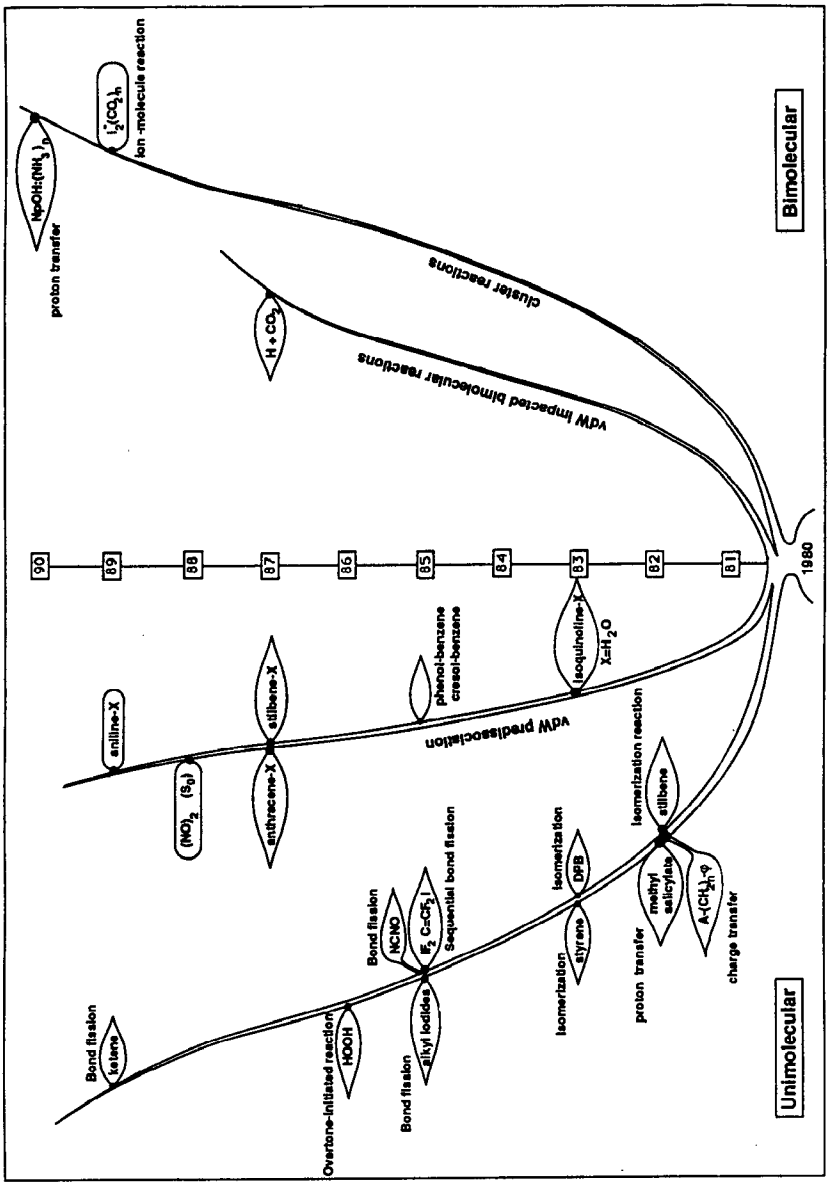

Figure 18b

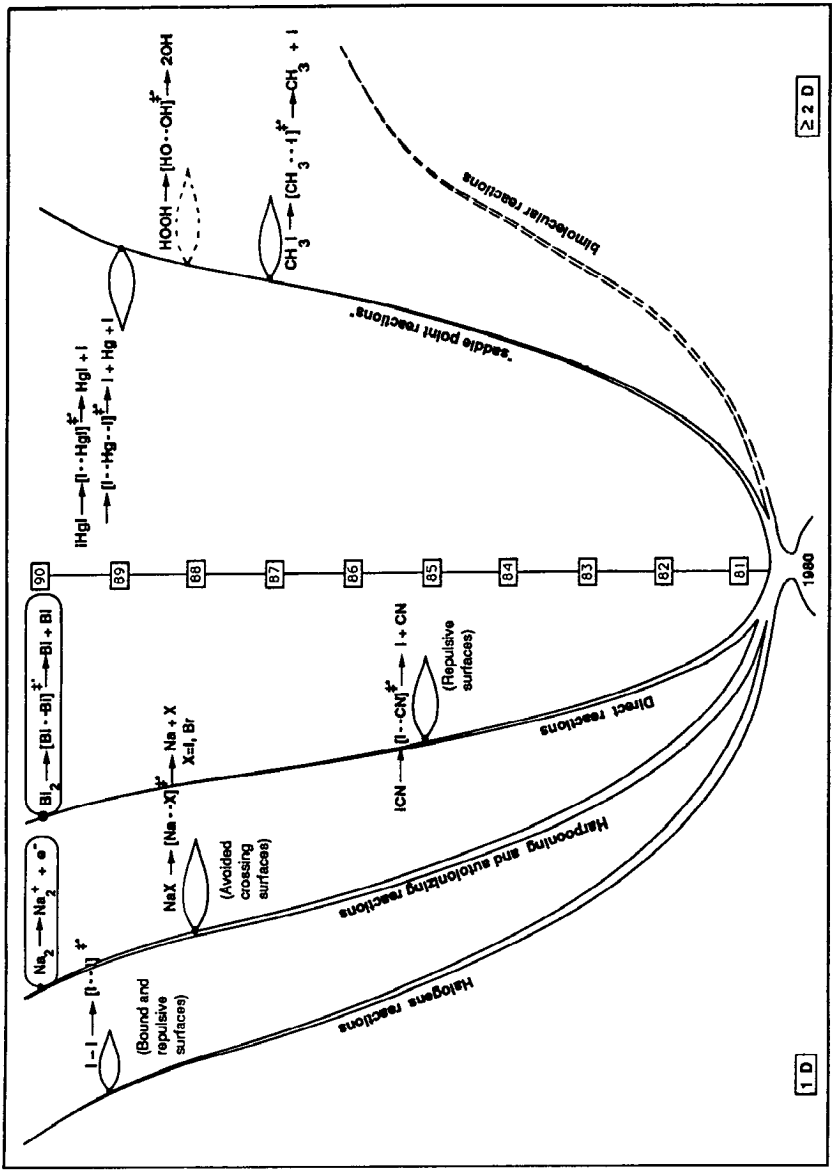

Figure 18c

states/cm^{-1}) to quasiexponential decays. A key feature in making the observations is the ability to excite the vibrational levels with a coherent pulse and to resolve the emission in frequency and in time (picoseconds). For rotational energy redistribution (and dephasing), an initial alignment is created and the temporal evolution is monitored. Rephasing of rotational motion was observed in polyatomics(!) and exploited to provide a Doppler-free method for determining excited state rotational constants in a number of systems. The concept of rotational energy scrambling in polyatomic molecules is not generally correct. Indeed, as in the case of vibrational energy redistribution, coherent (not chaotic) motion has been observed at relatively higher energies and even in reactive systems.

Picosecond photofragment spectroscopy has been applied to a number of elementary reactions. The time-resolution in these experiments is limited only by the pulse-widths; hence, microcanonical state-to-state rates can be measured directly. This advance allows us to map the microscopic dynamics, and together with product state distributions, critically test theories of unimolecular reactions, as illustrated in the text.

Femtosecond transition-state spectroscopy (FTS) has exposed transition-states of reactions in real-time. Since fragments move with a velocity typically 1 km$\cdot$s^{-1}, FTS provides a "shutter speed" of $\sim$0.01 Å/fs. So far, the elementary reactions studied involve "simple" quasi-bound surfaces, repulsive surfaces, surfaces with avoided crossings, and surfaces with two vibrational degrees-of-freedom. These real-time techniques have been extended to a special class of bimolecular reactions (e.g. $H+CO_2$), and more recently, to reactions in clusters. Femtosecond alignment experiments have also been successful.

Much more will be done in the coming years both in theory and in experiments. The general theme emerging is that the techniques and methodology in this field are now at a stage where it is possible to study reaction dynamics, from reagents to products (32, 33, 199–202), in real-time, from the picosecond to the femtosecond time scale ("femtochemistry"). With complementary energy (state) resolved techniques, we should now be able to obtain the fundamentals of the dynamics: the ultrashort time dynamics of transition states, the state-to-state rates, and the quantum state distributions in products. We hope that this article will stimulate many more studies, as indeed the number of new questions continues to grow—a healthy sign!

ACKNOWLEDGMENTS

Over the last ten years, this research was supported primarily by the National Science Foundation and the Air Force Office of Scientific Research, hereby gratefully acknowledged. The efforts and dedication of

a great number of graduate students and post-doctoral fellows, acknowledged in this review, have made this research possible. A.H.Z. wishes to thank R. A. Marcus, R. B. Bernstein, and R. Bersohn for many stimulating discussions; the fruits of some collaborations are acknowledged in the text. We are grateful to all our colleagues who provided us with preprints and reprints of their work. We hope that we were successful in including all relevant contributions and apologize to those whose work we did not have a chance to discuss.

L.R.K. would like to thank the National Research Council for support through a postdoctoral Resident Research Associateship at the Jet Propulsion Laboratory, Caltech, administered by the NASA.

Literature Cited

1. Levine, R. D., Bernstein, R. B. 1987. *Molecular Reaction Dynamics and Chemical Reactivity*. New York: Oxford Univ. Press
2. Pechukas, P. 1981. *Annu. Rev. Phys. Chem.* 32: 159
3. Truhlar, D. G., Hase, W. L., Hynes, J. T. 1983. *J. Phys. Chem.* 87: 2664
4. Herschbach, D. R. 1987. *Angew. Chem. Int. Ed. Engl.* 26: 1221
5. Lee, Y. T. 1987. *Angew. Chem. Int. Ed. Engl.* 26: 939
6. Polanyi, J. C. 1987. *Angew. Chem. Int. Ed. Engl.* 26: 952
7. Zare, R. N., Dagdigian, P. J. 1974. *Science* 185: 739
8. Bersohn, R. 1984. *J. Phys. Chem.* 88: 5145
9. Reisler, H., Wittig, C. 1986. *Annu. Rev. Phys. Chem.* 37: 307
10. Crim, F. F. 1984. *Annu. Rev. Phys. Chem.* 35: 657
11. Leone, S. R. 1984. *Annu. Rev. Phys. Chem.* 35: 109
12. Greene, C. H., Zare, R. N. 1982. *Annu. Rev. Phys. Chem.* 33: 119
13. Dzvonik, M., Yang, S., Bersohn, R. 1974. *J. Chem. Phys.* 61: 4408
14. Riley, S. J., Wilson, K. R. 1972. *Faraday Discuss. Chem. Soc.* 53: 132
15. Simons, J. P. 1987. *Molecular Photodissociation Dynamics*, ed. M. N. R. Ashfold, J. E. Baggott. *Adv. Gas-Phase Photochem. Kinet.* London: R. Soc. Chem.
16. Houston, P. L. 1987. *J. Phys. Chem.* 91: 5388
17. Gandhi, S. R., Curtiss, T. J., Bernstein, R. B. 1988. *Phys. Rev. Lett.* 59: 2951
18. Brooks, P. R. 1976. *Science* 193: 11
19. Bernstein, R. B., Herschbach, D. R., Levine, R. D., eds. 1987. *J. Phys. Chem.*, Vol. 91. No. 21. Special issue on *Dynamical Stereochemistry*
20. Levy, D. H., 1981. *Adv. Chem. Phys.* 47: 323 (Pt. 1)
21. Moore, C. B., Weisshaar, J. C. 1983. *Annu. Rev. Phys. Chem.* 34: 525 and refs. therein
22. Parmenter, C. S. 1983. *Faraday Discuss. Chem. Soc.* 75: 7 and refs. therein
23. Felker, P. M., Zewail, A. H. 1988. *Adv. Chem. Phys.* 70: 265 and refs. therein
24. Wardlaw, D. M., Marcus, R. A. 1988. *Adv. Chem. Phys.* 70: 231
25. Marcus, R. A. 1952. *J. Chem. Phys.* 20: 359
26. Marcus, R. A. 1965. *J. Chem. Phys.* 43: 2658
27. Pechukas, P., Light, J. C. 1965. *J. Chem. Phys.* 42: 3281
28. Pechukas, P., Light, J. C., Rankin, C. 1966. *J. Chem. Phys.* 44: 794
29. Quack, M., Troe, J. 1974. *Ber. Bunsenges. Phys. Chem.* 78: 240
30. Wardlaw, D. M., Marcus, R. A. 1985. *J. Chem. Phys.* 83: 3462
31. Wittig, C., Nadler, I., Reisler, H., Noble, M., Catanzarite, J., Radhakrishnan, G. 1985. *J. Chem. Phys.* 83: 5581
32. Zewail, A. H. 1988. *Science* 242: 1645, and refs. therein
33. Zewail, A. H., Bernstein, R. B. 1988. *C. & E. News*, Nov. 7, p. 24
34. Knee, J. L., Zewail, A. H. 1988. *Spectroscopy* 3: 44
35. Lambert, W. R., Felker, P. M., Zewail, A. H. 1981. *J. Chem. Phys.* 75: 5958
36. Felker, P. M., Zewail, A. H. 1983. *Chem. Phys. Lett.* 102: 113

37. Scherer, N. F., Doany, F. E., Zewail, A. H., Perry, J. W. 1986. *J. Chem. Phys.* 84: 1932
38. Knee, J. L., Khundkar, L. R., Zewail, A. H. 1985. *J. Chem. Phys.* 82: 4715
39. Dantus, M. D., Rosker, M. J., Zewail, A. H. 1987. *J. Chem. Phys.* 87: 2395
40. Shank, C. V. 1986. *Science* 233: 1276, and refs. therein
41. Zewail, A. H. 1980. *Phys. Today* 33(11): 27
42. Bloembergen, N., Zewail, A. H. 1984. *J. Phys. Chem.* 88: 5459
43. Butler, L. J., Hintsa, E. J., Shane, S. F., Lee, Y. T. 1987. *J. Chem. Phys.* 86: 2051
44. Felker, P. M., Zewail, A. H. 1984. *Phys. Rev. Lett.* 53: 501
45. Felker, P. M., Zewail, A. H. 1985. *J. Chem. Phys.* 82: 2961
46. Felker, P. M., Zewail, A. H. 1985. *J. Chem. Phys.* 82: 2975
47. Felker, P. M., Zewail, A. H. 1985. *J. Chem. Phys.* 82: 2994
48. Felker, P. M., Lambert, W. R., Zewail, A. H. 1985. *J. Chem. Phys.* 82: 3003
49. Peng, L. W., Keelan, B. W., Semmes, D. H., Zewail, A. H. 1988. *J. Phys. Chem.* 92: 5540
50. Semmes, D. H. 1989. PhD thesis. Calif. Inst. Technol., Pasadena
51. Syage, J. A., Felker, P. M., Semmes, D. H., Al Adel, F., Zewail, A. H. 1985. *J. Chem. Phys.* 82: 2896
52. Shepanski, J. F., Keelan, B. W., Zewail, A. H. 1983. *Chem. Phys. Lett.* 103: 9
53. Knee, J. L., Doany, F. E., Zewail, A. H. 1985. *J. Chem. Phys.* 82: 1042
54. Felker, P. M., Zewail, A. H. 1986. *Chem. Phys. Lett.* 128: 221
55. Novak, F., Kosloff, R., Tannor, D. J., Lorincz, A., Smith, D. D., Rice, S. A. 1985. *J. Chem. Phys.* 82: 1073
56. Knee, J. L., Khundkar, L. R., Zewail, A. H. 1985. *J. Phys. Chem.* 89: 3201
57. Felker, P. M., Zewail, A. H. 1983. *Chem. Phys. Lett.* 94: 448
58. Baskin, J. S., Dantus, M., Zewail, A. H. 1986. *Chem. Phys. Lett.* 130: 473
59. Baskin, J. S., Rose, T. S., Zewail, A. H. 1988. *J. Chem. Phys.* 88: 1458
60. Demmer, D. R., Hager, J. W., Leach, G. W., Wallace, S. C. 1987. *Chem. Phys. Lett.* 136: 329
61. Bickel, G. A., Demmer, D. R., Leach, G. W., Wallace, S. C. 1988. *Chem. Phys. Lett.* 145: 423
62. Wang, P.-N., Lim, E. C. 1987. *Chem. Phys. Lett.* 142: 389
63. Bickel, G. A., Demmer, D. R., Outhouse, E. A., Wallace, S. C. 1989. *J. Chem. Phys.* 91: 6013
64. Kaziska, A. J., Wittmeyer, S. A., Motyka, A. L., Topp, M. R. 1989. *Chem. Phys. Lett.* 154: 199
65. Lakshminarayan, C., Knee, J. L. 1989. *J. Phys. Chem.* 94: 2637
66. Schubert, U., Riedle, E., Neusser, H. J., Schlag, E. W. 1986. *J. Chem. Phys.* 84: 6182, and refs. therein
67. Kommandeur, J., Majewski, W. A., Meerts, W. L., Pratt, D. W. 1987. *Annu. Rev. Phys. Chem.* 38: 433
68. Siebrand, W., Meerts, W. L., Pratt, D. W. 1989. *J. Chem. Phys.* 90: 1313
69. Nadler, W., Marcus, R. A. 1987. *J. Chem. Phys.* 86: 6982
70. Nadler, W., Marcus, R. A. 1988. *Chem. Phys. Lett.* 144: 509
71. Shan, K., Yan, Y. J., Mukamel, S. 1987. *J. Chem. Phys.* 87: 2021
72. Mukamel, S. 1988. *Adv. Chem. Phys.* 70: 165
73. Felker, P. M., Zewail, A. H. 1987. *J. Chem. Phys.* 86: 2460
74. Baskin, J. S., Felker, P. M., Zewail, A. H. 1987. *J. Chem. Phys.* 86: 2483
75. Felker, P. M., Baskin, J. S., Zewail, A. H. 1986. *J. Phys. Chem.* 90: 724
76. Baskin, J. S., Zewail, A. H. 1989. *J. Phys. Chem.* 93: 5701
77. Myers, A. B., Hochstrasser, R. M. 1986. *J. Chem. Phys.* 85: 6301, and refs. therein
78. Scherer, N. F., Khundkar, L. R., Rose, T. S., Zewail, A. H. 1987. *J. Phys. Chem.* 91: 6478
79. Cote, M. J., Kauffman, J. F., Smith, P. G., McDonald, J. D. 1989. *J. Chem. Phys.* 90: 2865
80. Kauffman, J. F., Cote, M. J., Smith, P. G., McDonald, J. D. 1989. *J. Chem. Phys.* 90: 2874
81. Riedle, E., Neusser, H. J., Schlag, E. W., Lin, S. H. 1984. *J. Phys. Chem.* 88: 198
82. Nathanson, G. M., McClelland, G. M. 1984. *J. Chem. Phys.* 81: 629
83. Lambert, W. R., Felker, P. M., Zewail, A. H. 1984. *J. Chem. Phys.* 81: 2217
84. Amirav, A., Jortner, J., Terazima, M., Lim, E. C. 1987. *Chem. Phys. Lett.* 133: 179
85. Zewail, A. H. 1989. *J. Chem. Soc. Faraday Trans. 2* 85: 1221
86. Dantus, M., Bowman, R. M., Baskin, J. S., Zewail, A. H. 1989. *Chem. Phys. Lett.* 159: 406
87. Hasselbrink, E., Waldeck, J. R., Zare, R. N. 1988. *Chem. Phys.* 126: 191
88. O'Halloran, M. A., Joswig, H., Zare, R. N. 1987. *J. Chem. Phys.* 87: 303
89. Hall, G. E., Sivakumar, N., Houston,

P. L. 1986. *J. Chem. Phys.* 84: 2120
90. Nadler, I., Mahgerefteh, D., Reisler, H., Wittig, C. 1985. *J. Chem. Phys.* 82: 3885
91. Marinelli, W. J., Sivakumar, N., Houston, P. L. 1984. *J. Phys. Chem.* 88: 6685
92. Baskin, J. S., Semmes, D., Zewail, A. H. 1986. *J. Chem. Phys.* 85: 7488
93. Robinson, P. J., Holbrook, K. A. 1972. *Unimolecular Reactions.* New York: Wiley
94. Forst, W. 1973. *Theory of Unimolecular Reactions.* New York: Academic
95. Pollak, E. 1985. In *Theory of Chemical Reaction Dynamics*, ed. M. Baer. Boca Raton, Fl: CRC Press
96. Clary, D. C., ed. 1985. *Theory of Chemical Reactions.* NATO ASI Ser. C, 170. Boston: Reidel
97. Chesnavich, W. J., Bowers, M. T. 1977. *J. Chem. Phys.* 66: 2306
98. Dumont, R. S., Brumer, P. 1986. *J. Phys. Chem.* 90: 3509
99. Nadler, I., Noble, M., Reisler, H., Wittig, C. 1985. *J. Chem. Phys.* 82: 2608
100. Nadler, I., Pfab, J., Reisler, H., Wittig, C. 1984. *J. Chem. Phys.* 81: 653
101. Qian, C. X. W., Noble, M., Nadler, I., Reisler, H., Wittig, C. 1985. *J. Chem. Phys.* 83: 5573
102. Qian, C. X. W., Ogai, A., Reisler, H., Wittig, C. 1989. *J. Chem. Phys.* 90: 209
103. Khundkar, L. R., Knee, J. L., Zewail, A. H. 1987. *J. Chem. Phys.* 87: 77
104. Bai, Y. Y., Segal, G. A. 1988. *Chem. Phys. Lett.* 151: 31
105. Dupuis, M., Lester, W. A. Jr. 1985. *J. Chem. Phys.* 83: 3990
106. Troe, J. 1988. *Ber. Bunsenges. Phys. Chem.* 92: 242
107. Klippenstein, S. J., Khundkar, L. R., Zewail, A. H., Marcus, R. A. 1988. *J. Chem. Phys.* 89: 4761
108. Reddy, K. V., Berry, M. J. 1977. *Chem. Phys. Lett.* 52: 111
109. Chuang, M. C., Baggott, J. E., Chandler, D. W., Farneth, W. E., Zare, R. N. 1983. *Faraday Discuss. Chem. Soc.* 75: 301
110. Natzle, W. C., Moore, C. B., Goodall, D. M., Frisch, W., Holzwarth, J. F. 1981. *J. Phys. Chem.* 85: 2882
111. Rizzo, T. R., Hayden, C. C., Crim, F. F. 1983. *Faraday Discuss. Chem. Soc.* 75: 223
112. Ticich, T. M., Rizzo, T. R., Dübal, H. R., Crim, F. F. 1986. *J. Chem. Phys.* 84: 1508
113. Likar, M. D., Baggott, J. E., Crim, F. F. 1989. *J. Chem. Phys.* 90: 6266
114. Ticich, T. M., Likar, M. D., Dübal, H. R., Butler, L. J., Crim, F. F. 1987. *J. Chem. Phys.* 87: 5820
115. Brouwer, L., Cobos, C. J., Troe, J., Dübal, H.-R., Crim, F. F. 1987. *J. Chem. Phys.* 86: 6171
116. Scherer, N. F., Zewail, A. H. 1987. *J. Chem. Phys.* 87: 97
117. Chen, I.-C., Green, W. H. Jr., Moore, C. B. 1988. *J. Chem. Phys.* 89: 314
118. Bitto, H., Chen, I.-C., Moore, C. B. 1986. *J. Chem. Phys.* 85: 5101
119. Potter, E. D., Gruebele, M., Khundkar, L. R., Zewail, A. H. 1989. *Chem. Phys. Lett.* 164: 463
120. Klippenstein, S. J., Marcus, R. A. 1989. *J. Chem. Phys.* 91: 2280
121. Knee, J. L., Khundkar, L. R., Zewail, A. H. 1985. *J. Chem. Phys.* 83: 1996
122. Khundkar, L. R., Zewail, A. H. 1990. *J. Chem. Phys.* 92: 231
123. Knee, J. L., Khundkar, L. R., Zewail, A. H. 1987. *J. Chem. Phys.* 87: 115
124. Semmes, D. H., Baskin, J. S., Zewail, A. H. 1990. *J. Chem. Phys.* 92: 3359
125. Semmes, D. H., Baskin, J. S., Zewail, A. H. 1987. *J. Am. Chem. Soc.* 109: 4104
126. Syage, J. A., Felker, P. M., Zewail, A. H. 1984. *J. Chem. Phys.* 81: 4706
127. Felker, P. M., Lambert, W. R., Zewail, A. H. 1982. *J. Chem. Phys.* 77: 1603
128. Syage, J. A., Felker, P. M., Zewail, A. H. 1984. *J. Chem. Phys.* 81: 2233
129. Ramaekers, J. J. F., van Dijk, H. K., Langelaar, J., Rettschnick, R. P. H. 1983. *Faraday Discuss. Chem. Soc.* 75: 183
130. Weber, P. M., Rice, S. A. 1988. *J. Chem. Phys.* 88: 6120
131. Casassa, M. P., Stephenson, J. C., King, D. S. 1988. *J. Chem. Phys.* 89: 1966
132. Janda, K. C. 1985. *Adv. Chem. Phys.* 60: 201
133. Miller, R. E. 1986. *J. Phys. Chem.* 90: 3301
134. Foth, H. J., Polanyi, J. C., Telle, H. H. 1982. *J. Phys. Chem.* 86: 5027
135. Imre, D., Kinsey, J. L., Sinha, A., Krenos, J. 1984. *J. Phys. Chem.* 88: 3956
136. Brooks, P. R., Curl, R. F., Maguire, T. C. 1982. *Ber. Bunsenges. Phys. Chem.* 86: 401
137. Brooks, P. R. 1988. *Chem. Rev.* 88: 407
138. Nieh, J.-C., Valentini, J. J. 1988. *Phys. Rev. Lett.* 60: 519
139. Metz, R. B., Kitsopoulos, T., Weaver, A., Neumark, D. M. 1988. *J. Chem. Phys.* 88: 1463

140. Scherer, N. F., Knee, J. L., Smith, D. D., Zewail, A. H. 1985. *J. Phys. Chem.* 89: 5141
141. Dantus, M., Rosker, M. J., Zewail, A. H. 1987. *J. Chem. Phys.* 87: 2395
142. Rosker, M. J., Dantus, M., Zewail, A. H. 1988. *J. Chem. Phys.* 89: 6113
143. Dantus, M., Rosker, M. J., Zewail, A. H. 1988. *J. Chem. Phys.* 89: 6128
144. Rosker, M. J., Dantus, M., Zewail, A. H. 1988. *Science* 241: 1200
145. Bernstein, R. B., Zewail, A. H. 1989. *J. Chem. Phys.* 90: 829
146. Bersohn, R., Zewail, A. H. 1988. *Ber. Bunsenges. Phys. Chem.* 92: 373
147. Heller, E. J. 1981. *Acc. Chem. Res.* 14: 368
148. Williams, S. O., Imre, D. G. 1988. *J. Phys. Chem.* 92: 6648
149. Benjamin, I., Wilson, K. R. 1989. *J. Chem. Phys.* 90: 4176
150. Heather, R., Metiu, H. 1989. *Chem. Phys. Lett.* 157: 505
151. Henricksen, N. E., Heller, E. J. 1989. *J. Chem. Phys.* 91: 4700
152. Yan, Y. J., Fried, L. E., Mukamel, S. 1989. *J. Phys. Chem.* 93: 8149
153. Krause, J. L., Shapiro, M., Bersohn, R. *J. Chem. Phys.* Submitted
154. Kono, H., Fujimura, Y. 1989. *J. Chem. Phys.* 91: 5960
155. Yamashita, K., Morokuma, K. 1989. *J. Chem. Phys.* 91: 7477
156. Rose, T. S., Rosker, M. J., Zewail, A. H. 1989. *J. Chem. Phys.* 91: 7415
157. Rose, T. S., Rosker, M. J., Zewail, A. H. 1988. *J. Chem. Phys.* 88: 6672
158. Rosker, M. J., Rose, T. S., Zewail, A. H. 1988. *Chem. Phys. Lett.* 146: 175
159. Lee, S. Y., Pollard, W. T., Mathies, R. A. 1989. *J. Chem. Phys.* 90: 6146
160. Marcus, R. A. 1988. *Chem. Phys. Lett.* 152: 8
161. Fried, L. E., Mukamel, S. *J. Chem. Phys.* Submitted
162. Engel, V., Metiu, H., Almeida, R., Marcus, R. A., Zewail, A. H. 1988. *Chem. Phys. Lett.* 152: 1
163. Engel, V., Metiu, H. 1989. *J. Chem. Phys.* 90: 6116; *J. Chem. Phys.* 91: 1596
164. Choi, S. E., Light, J. C. 1989. *J. Chem. Phys.* 90: 2593
165. Lin, S. H., Fain, B. 1989. *Chem. Phys. Lett.* 155: 216
166. Bowman, R. M., Dantus, M., Zewail, A. H. 1989. *Chem. Phys. Lett.* 161: 297
167. Dantus, M., Bowman, R. M., Zewail, A. H. 1990. *Nature* 343: 737
168. Gruebele, M., Roberts, G., Dantus, M., Bowman, R. M., Zewail, A. H. 1990. *Chem. Phys. Lett.* 166: 459
169. Dantus, M., Bowman, R. M., Gruebele, M., Zewail, A. H. 1989. *J. Chem. Phys.* 91: 7437
170. Bowman, R. M., Dantus, M., Zewail, A. H. 1989. *Chem. Phys. Lett.* 156: 131
171. Khundkar, L. R., Zewail, A. H. 1987. *Chem. Phys. Lett.* 142: 426
172. Knee, J. L., Khundkar, L. R., Zewail, A. H. 1985. *J. Chem. Phys.* 83: 1996
173. Scherer, N. F. 1989. PhD thesis. Calif. Inst. Technol., Pasadena
174. Jouvet, C., Soep, B. 1983. *Chem. Phys. Lett.* 96: 426
175. Jouvet, C., Boivineau, M., Duval, M. C., Soep, B. 1987. *J. Phys. Chem.* 91: 5416
176. Buelow, S., Radhakrishnan, G., Catanzarite, J., Wittig, C. 1985. *J. Chem. Phys.* 83: 444
177. Buelow, S., Radhakrishnan, G., Wittig, C. 1987. *J. Phys. Chem.* 91: 5409
178. Oldershaw, G. A., Porter, D. A. 1969. *Nature* 223: 490
179. Tomalesky, R. E., Sturm, J. E. 1972. *J. Chem. Soc. Faraday Trans. 2* 68: 1241
180. Quick, C. R. Jr., Tiee, J. J. 1983. *Chem. Phys. Lett.* 100: 223
181. Kleinermanns, K., Wolfrum, J. 1984. *Chem. Phys. Lett.* 104: 157
182. Kleinermanns, K., Wolfrum, J. 1983. *Laser Chem.* 2: 339
183. Kleinermanns, K., Linnebach, E., Wolfrum, J. 1985. *J. Phys. Chem.* 89: 2525
184. Jacobs, A., Wahl, M., Weller, R., Wolfrum, J. 1989. *Chem. Phys. Lett.* 158: 161
185. Milligan, D. E., Jacox, M. E. 1971. *J. Chem. Phys.* 54: 927
186. Jacox, M. E. 1988. *J. Chem. Phys.* 88: 4598
187. McLean, A. D., Ellinger, Y. 1985. *Chem. Phys.* 94: 25
188. Smith, I. W. M., Zellner, R. 1973. *J. Chem. Soc. Faraday Trans 2* 69: 1617
189. Smith, I. W. M. 1977. *Chem. Phys. Lett.* 49: 112
190. Brunning, J., Derbyshire, D. W., Smith, I. W. M., Williams, M. D. 1988. *J. Chem. Soc. Faraday Trans. 2* 84: 105
191. Larson, C. W., Stewart, P. H., Golden, D. M. 1988. *Int. J. Chem. Kinet.* 20: 27
192. Mozurkewich, M., Lamb, J. J., Benson, S. W. 1984. *J. Phys. Chem.* 88: 6435
193. Schatz, G. C., Fitzcharles, M. S., Harding, L. B. 1987. *Faraday Discuss. Chem. Soc.* 84: 359
194. Schatz, G. C., Fitzcharles, M. S. 1988. In *Selectivity in Chemical Reactions*, ed. J. C. Whitehead, p. 353. Dordrecht: Kluwer Acad. Publ.

195. Scherer, N. F., Khundkar, L. R., Bernstein, R. B., Zewail, A. H. 1987. *J. Chem. Phys.* 87: 1451
196. Scherer, N. F., Sipes, C. N., Bernstein, R. B., Zewail, A. H. 1990. *J. Chem. Phys.* 92: 5239
197. Breen, J. J., Peng, L. W., Wilberg, D., Cong, P., Heikal, A., Zewail, A. H. 1990. *J. Chem. Phys.* 92: 805
198. Ray, D., Levinger, N. E., Papanikolas, J. M., Lineberger, W. C. 1989. *J. Chem. Phys.* 91: 6533
199. Smith, I. W. M. 1987. *Nature* 328: 760
200. Baggott, J. 1989. *New Sci.* 122: 58
201. Zare, R. N. 1990. *Laser Photochemistry, McGraw Hill Year Book of Science and Technology*. In press
202. Smith, I. W. M. 1990. *Nature* 343: 691
203. Smith, P. G., McDonald, J. D. 1990. *J. Chem. Phys.* 92: 1004
204. Connell, L. L., Corcoran, T. C., Joireman, P. W., Felker, P. M. 1990. *J. Phys. Chem.* 94: 1229
205. Shepanski, J. F., Keelan, B. W., Zewail, A. H. 1983. *Chem. Phys. Lett.* 103: 9
206. Syage, J. A., Al-Adel, F., Zewail, A. H. 1983. *Chem. Phys. Lett.* 103: 15
207. Felker, P. M., Zewail, A. H. 1983. *J. Chem. Phys.* 78: 5266
208. Nimlos, M. R., Young, M. A., Bernstein, E. R., Kelley, D. F. 1989. *J. Chem. Phys.* 91: 5268
209. Glownia, J. H., Misewich, J. A., Sorokin, P. P. 1990. *J. Chem. Phys.* 92: 3335
210. Baumert, T., Bühler, B., Thalweiser, R., Gerber, G. 1990. *Phys. Rev. Lett.* 64: 733

Annual Review of Physical Chemistry
Volume 41, 1990

CONTENTS

(*continued*) vii